BEHAVIOUR OF AXIALLY LOADED TUBULAR V-JOINTS

by

SANDRO SCOLA

Department of Civil Engineering and Applied Mechanics
McGill University
Montreal, Canada

March 1989

A thesis submitted to the Faculty of Graduate Studies and Research in partial fulfillment of the requirements for the degree of Master of Engineering

It was the best of times,

It was the worst of times,

It was a long, long time,

But it was not a waste of time.

To my parents

ABSTRACT

The results of an experimental test program on axially loaded tubular joints comprising eigth V-joints, six T-joints and one DT-joints are reported. The behaviour of the joints is described by their ultimate strenghts load-deformation characteristics, and stress concentration factors. Comparaisons are made to study the effect of beta,gamma,and phi on the joints response. Comparable T and V specimens are examined and it is found that the addition of an out-of-plane branch may, in certain situations, alter the T-joint behaviour in such a way that the common practice of treating a V-joint as two separate T-joints may be unsafe.

A Finite Element package called TUBE ANALYSIS SYSTEM (TAS) is developped. The package consist of a 2D main core processor as well as pre and post graphical processors. Predictions are compared favourably with most V-joints experimental results but generally less successfully with T-joints results.

RESUME

Les résultats d'un programme expérimental portant sur les joints tubulaires chargés axiallement et comprenant huit joints-V, six joints-T, et un joint-DT sont rapportés. Le comportement des joints est décrit par leurs capacités ultime, caractéristiques charge-déformation, et coefficients de concentration de contrainte. Des comparaisons sont éffectuées pour étudier les effets du ratio de diamètre, β, du ratio d'épaisseur de la membrure, γ, et de l'angle hors-plan, ϕ, sur la réponse des joints. Des spécimens de joint-T et de joint-V comparables sont étudiés et il est montré que l'addition d'une entretoise hors-plan peut, en certaines occasions, altérer le comportement d'un joint-T de façon à ce que la pratique commune qui consiste à traiter un joint-V comme deux joints-T individuel devienne non-sécuritaire.

Un système à éléments finis appellé TUBE ANALYSIS SYSTEM (TAS) est développé. Le système comprend un programme d'analyse central en deux dimensions supportés par des pré- et post-processeurs graphiques. Les prédictions analytiques sont comparées favorablement avec les résultats de joints-V. Les comparaisons avec les résultats de joint-T sont cependant moins favorables.

ACKNOWLEDGEMENTS

The author would like to take this oppurtunity to thanks his research directors, Professors R.G. Redwood and H. Mitri, for their guidance, support, and patience throughout this research program.

In addition the author wishes to thank the Civil Engineering Department of McGill university for the use of their testing and computer facilities. The author is particularly grateful for the assistance given by B. Cockayne and R. Sheppard during the experimental phase and Dr. W.D. Cook during the development of the computer package.

The authors wishes to express his sincere gratitude to his parents for their never ending support and encouragements.

Thanks are also extended to my colleagues, past and present, of Room 498 for informative discussions and moral support.

The financial assistance provided by the Natural Sciences and Engineering Research Council of Canada is gratefully acknowledged.

The efforts of Andrew Ng in expertly typestting this manuscript are greatly appreciated.

TABLE OF CONTENTS

TABLE OF CONTENTS *(Continued)*

LIST OF FIGURES

LIST OF FIGURES *(Continued)*

LIST OF TABLES

LIST OF SYMBOLS

A	Area
A_i	Strain gauge location
[B]	Strain matrix
B_i	Strain gauge location
d	Branch diameter
D	Chord diameter
E	Modulus of elasticity
E_T	Tangent modulus
G	Shear modulus
I	Moment of inertia
$[K^t]$	Total element stiffness matrix
$[K_{sp}]$	Spring element stiffness matrix
$[K_{NAF}]$	Element stiffness matrix from NAF2D
K_n	Normal spring constant
K_t	Tangential spring constant
L	Unsupported chord length
L_e	Element length
N	Shape functions
P	Applied load
P_u	Ultimate load
P_y	Yield load
r	Branch radius
R	Chord radius
{R}	Consitent load vector
Q_β	Geometric modifier
t	Branch thickness
T	Chord thickness
T_e	Element thickness
W_e	Element width
u_i	Node i degree-of-freedom in the x-direction

LIST OF SYMBOLS *(Continued)*

v_i	Node i degree-of-freedom in the y-direction
Z	$(L/(RT))^{\frac{1}{2}}$
α	Chord length parameter
α_o	Chord ovalizing parameter
η	V-joint to T-joint Stress Concentration Factor ratio
β	Diameter ratio
σ_u	Ultimate stress
σ_y	Yield stress
ε	Strain
γ	Chord thinness ratio
τ	Wall thickness ratio
μ	V-joint to T-joint strength ratio
ϕ	Included out-of-plane angle between two branches
θ	Included in-plane angle between chord and branch
θ_i	Node i degree-of-freedom in the z-direction
$\{\Delta\}$	Nodal displacement vector
$\{\psi\}$	Unbalanced load vector
ΔW	Out of balance force

CHAPTER 1
INTRODUCTION

1.1 Introduction

Circular tubes possess characteristics that have contributed to their extensive use in offshore steel structures over the last three decades. Their high strength to weight ratio makes them structurally efficient and their high buoyancy and low drag coefficient facilitate transportation and reduce wave forces. These positive characteristics are counterbalanced by the difficulties which lie in the design and fabrication of tubular joints. The recognition of these difficulties led to world-wide research efforts as well as the development of many design codes. The most comprehensive review of both research work and design codes is contained in a 1985 report of the U.K. Underwater Engineering Group (UEG)[1].

The research work, both experimental and theoretical, has generally been aimed at increasing the designers' understanding of the behaviour of the planar joints such as the T, K, Y, DT and X-joints shown in Fig. 1.1. The more complex multiplanar joints have historically been treated as a series of uniplanar joints. At the present time design codes usually provide guidance on reducing the problem of a multiplanar joint to that of a simple planar joint. V-joints for example can be viewed as two T-joints separated by an angle ϕ as shown in Fig. 1.2. Figure 1.2 also identifies the important parameters influencing the strength of a tubular joint. The aim of this study is to

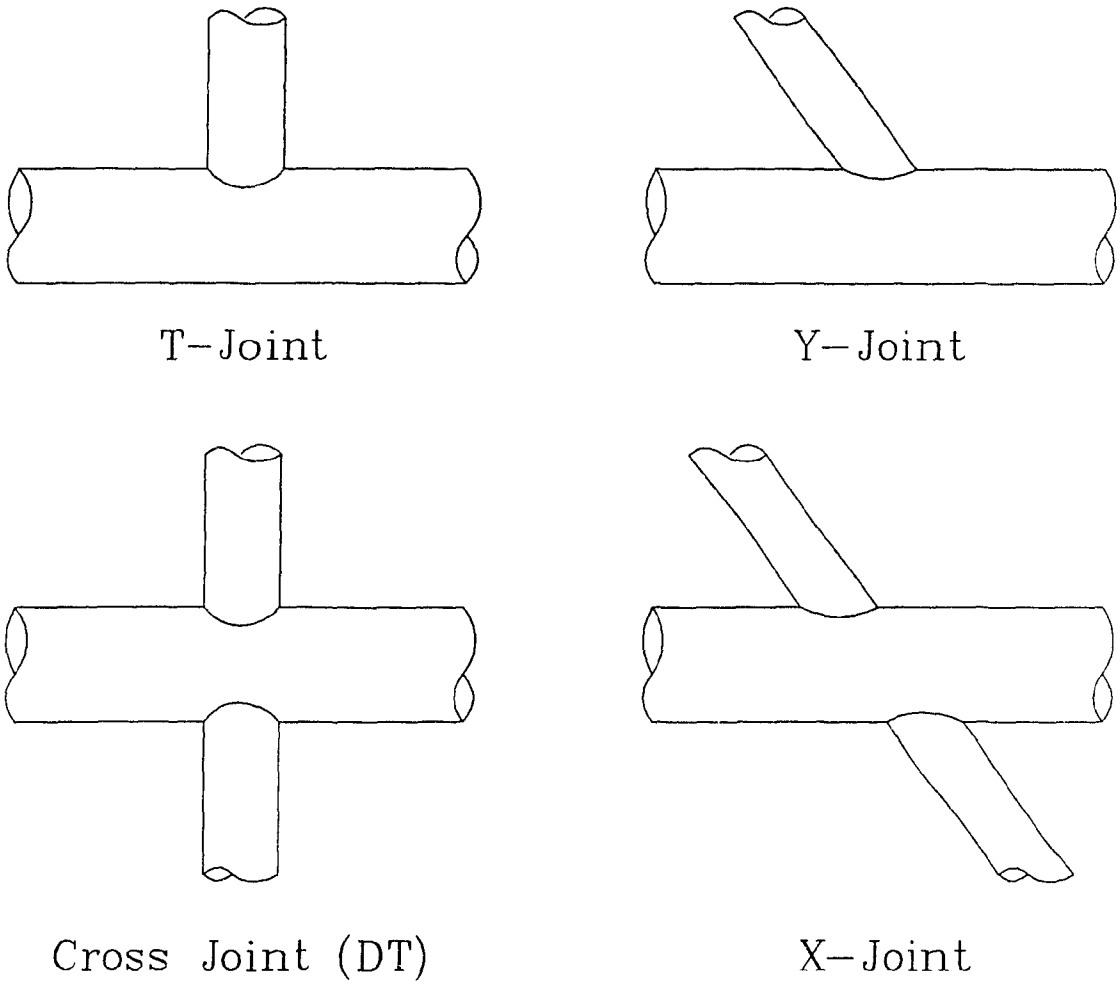

Figure 1.1 Geometrical Classification of Simple Planar Joint.

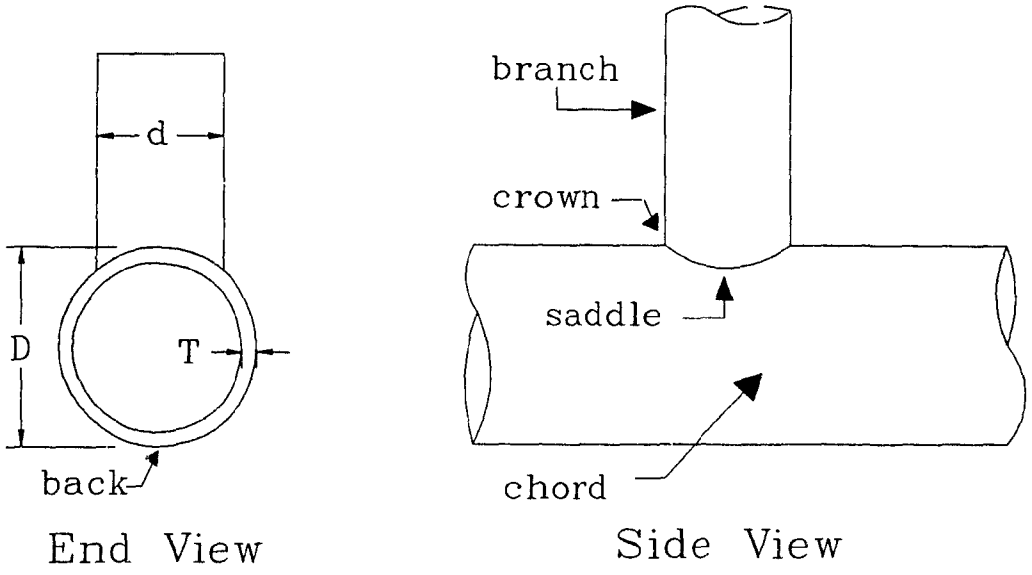

(a) T-joint

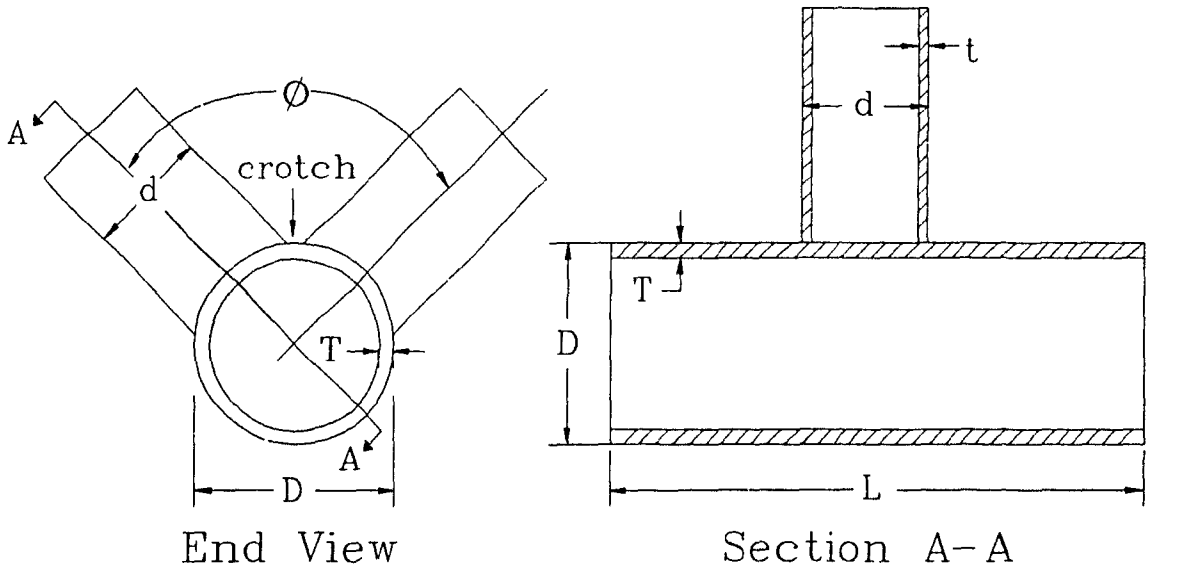

$$\gamma = D/2T \qquad \alpha = 2L/D \qquad \tau = t/T \qquad \beta = d/D$$

(b) V-joint

Figure 1.2 Joint Nomenclature.

examine the behaviour of a simple multiplanar joint, the V-joint, with the objective of either confirming the validity of treating such a joint as equivalent to two planar joints or establishing new guidelines for the design of V-joints.

1.2 Literature Review

As indicated above, most of the research work to date has been concerned with simple planar joints. Although the focus of this thesis is on V-joints, little information is available about such joints, and this section will therefore primarily examine publications concerned with T-joints.

Research on T-joints has been focused on two areas. These are:

(1) stress prediction and in particular hotspot stress calculations for use in fatigue design, where the hotspot stress is defined as the maximum stress near the weld toe but excluding the influence of notch stresses and,

(2) development of ultimate strength equations.

Different theoretical and experimental approaches have been used. Theoretical investigations have included thin shell theory and the finite element method (FEM) whereas experimental tests have been performed on steel, acrylic, and photoelastic models.

The first general theory of shells was proposed by Love in 1888. Donnell in 1934, and Flugge in 1955 developed the basic thin shell equations which were used in most of the early analytical studies[1,2]. By 1966 Toprac, Johnston, and Noel[3] reported that Flugge's equations as solved by Bijlaard represented the most accurate means of estimating peak stresses in the welded region of a tubular joint. It was pointed out that the solution had two major shortcomings. Firstly the branch load was approximated by a rectangular uniformly loaded pad and, secondly, the interaction of the relative stiffness of the two tubes was neglected.

Many references[1,4,5] report a more complete treatment by Dundrova. Her analyses combined a full shell representation of the chord with a membrane representation of

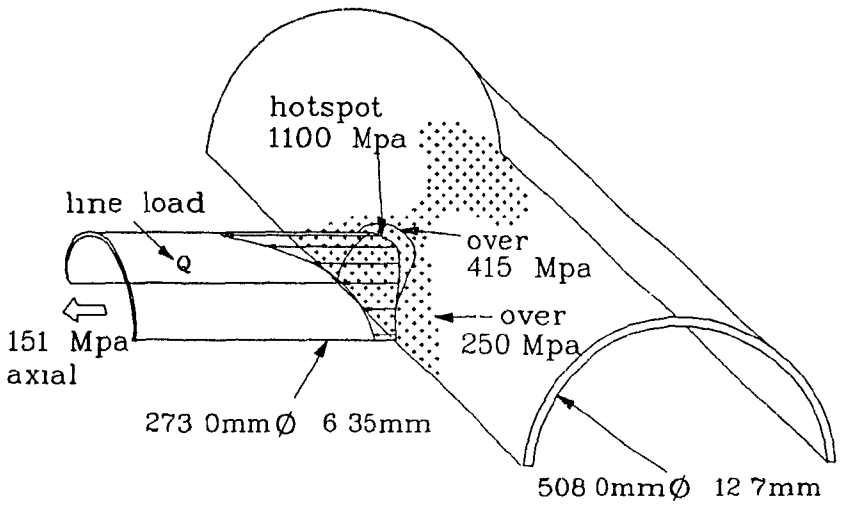

Figure 1.3 Dundrova Elastic Stress Distribution[6].

the branch. Results for a typical joint as given by Graff, Marshall and Nimas[6] are shown in Fig. 1.3. Although this analysis did not completely model the branch-chord connection, it was the first time that the branch was explicitly included in the solution

In 1970, Scordelis and Bouwkamp[2] used a computer program based on Donnell's equation to model a T-joint as a simply supported chord subjected to a uniform deflection at the branch-chord intersection. Although this model was not as theoretically sound as Dundrova's, the assumed deflection pattern produced a realistic load distribution on the chord (Fig. 1.4).

A full formulation of stress distribution in both branch and chord was presented by Chen, Chen, and Wang[7] in 1983. The intersection line was discretized into a finite number of points but both the branch and chord were treated as integrated shells. Comparisons with Kuang et al's[5] finite element analysis solution appeared to yield satisfactory agreement.

Notwithstanding recent developments, classical thin shell theory has not become a standard tool for the analysis of tubular connections. This is due to its mathematical complexity and to the fact that it is based on linear elasticity and consequently cannot

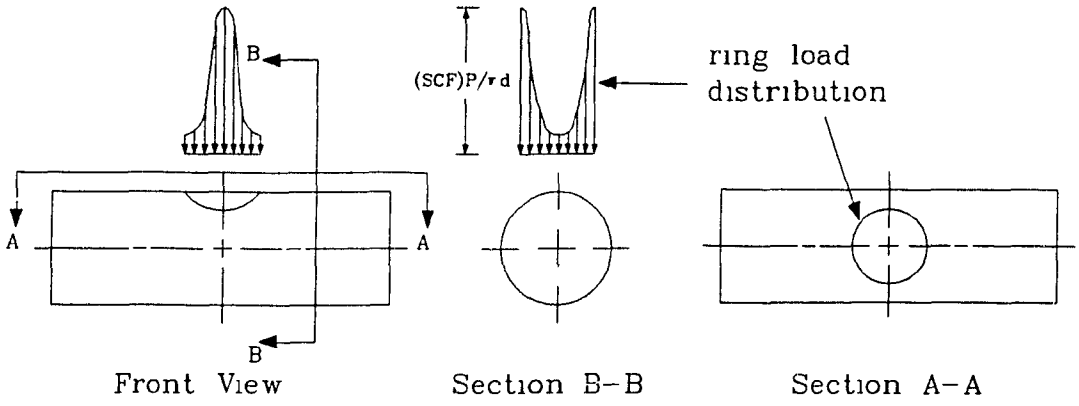

Figure 1.4 Analytical Model used by Scordelis.

be extended to investigate joint behaviour beyond the point of first yield.

The finite element method (FEM) is generally considered as the most practical numerical technique for tubular joint analysis[1,8]. The versatility of the method permits modelling of complex geometries, boundary conditions, and nonlinear material properties. The FEM first emerged as a leading analysis method in the mid-sixties following advances in computer hardware and publication of appropriate shell elements. Advances in hardware, programming, and element formulation have been almost continuous since then.

In the 1970's linear elastic FEM programs were used to predict hotspot stresses and calculate the ratio of hotspot stress to nominal branch stress i.e. stress concentration factors (SCF)[5,9,10]. Parametric studies were then performed to propose SCF equations. The Reber[11] and Visser[9] equations for a T-joint loaded in uniaxial compression are listed in Table 1.1. More complete parametric studies were carried out by Kuang, Potvin, and Leick[5] in 1975 and Gibstein[10] in 1978. Their research produced SCF equations for both branch and chord. Kuang et al's formulae were cited in API RP2A[12] as being appropriate. Kuang et al's 1977 update and Gibstein formulae are both given in Table 1.1

Table 1.1 Stress Concentration Factors for Axially Loaded T-joints*

Reber[11] 1972	$SCF = 2.95\beta^{-0.1}\gamma^{0.6}\tau$	
Visser[9] 1974	$SCF = \tau(10 + 0.3\gamma)(1.4 - 0.75\beta)$	
Kuang et al[5] 1977	$SCF_C = 1.981\alpha^{0.057}e^{-1.2\beta^3}\gamma^{0.808}\tau^{1.333}$	$7 \le \alpha \le 40$
	$SCF_B = 3.751\alpha^{0.12}e^{-1.3\beta^3}\gamma^{0.55}\tau$	$0.3 \le \beta \le 0.8$
		$8.3 \le \gamma \le 33.3$
		$0.2 \le \tau \le 0.8$
Gibstein[10] 1978	$SCF_C = \alpha^{0.06}[1.44 - 3.72(\beta - 0.47)^2]\gamma^{0.87}\tau^{1.37}$	$7 \le \alpha \le 16$
		$0.225 \le \beta \le 0.9$
		$10 \le \gamma \le 30$
		$0 \le \tau \le 1.0$
	$SCF_B = \alpha^{0.12}[1 - 1.78(\beta - 0.5)^2]\gamma^{0.76}\tau^{0.57}$	$7 \le \alpha \le 16$
		$0.3 \le \beta \le 0.9$
		$10 \le \gamma \le 30$
		$0.47 \le \tau \le 1.0$
Wordsworth and	$SCF_C = \beta\gamma\tau(6.78 - 6.42\beta^{0.5})$	$8 \le \alpha \le 40$
Smedley[28] 1978	$SCF_B = 1 + 0.63SCF_c$	$0.13 \le \beta \le 1.0$
		$12 \le \gamma \le 32$
		$0.2 \le \tau \le 1.0$

* The hotspot for axially loaded T-joints is located at the chord-branch saddle.

The FEM programs of the 1980's use a variety of shell elements. However, curved thin shell elements such as Irons[13] isoparametric Semiloof element (Fig. 1.5) have been most popular in the analysis of tubular T-joints.

The 1980's have seen the introduction of non-linearity in shell elements and consequently attempts to predict the full load-deflection curve of T-joints. A program called Lusas, which uses an improved 32 d.o.f. Semiloof shell element, was developed at Kingston Polytechnic. It was reported by Stamenkovic and Sparrow[14] that the results seemed promising. Figure 1.6 shows the results of a typical run as presented by Brebbia[15].

With the continuous improvements in element formulation as well as the increasing

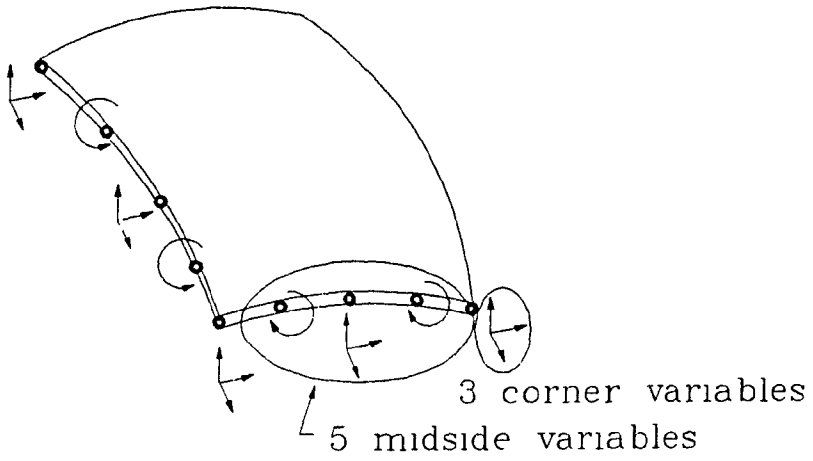

Figure 1.5 Semiloof Shell Element.

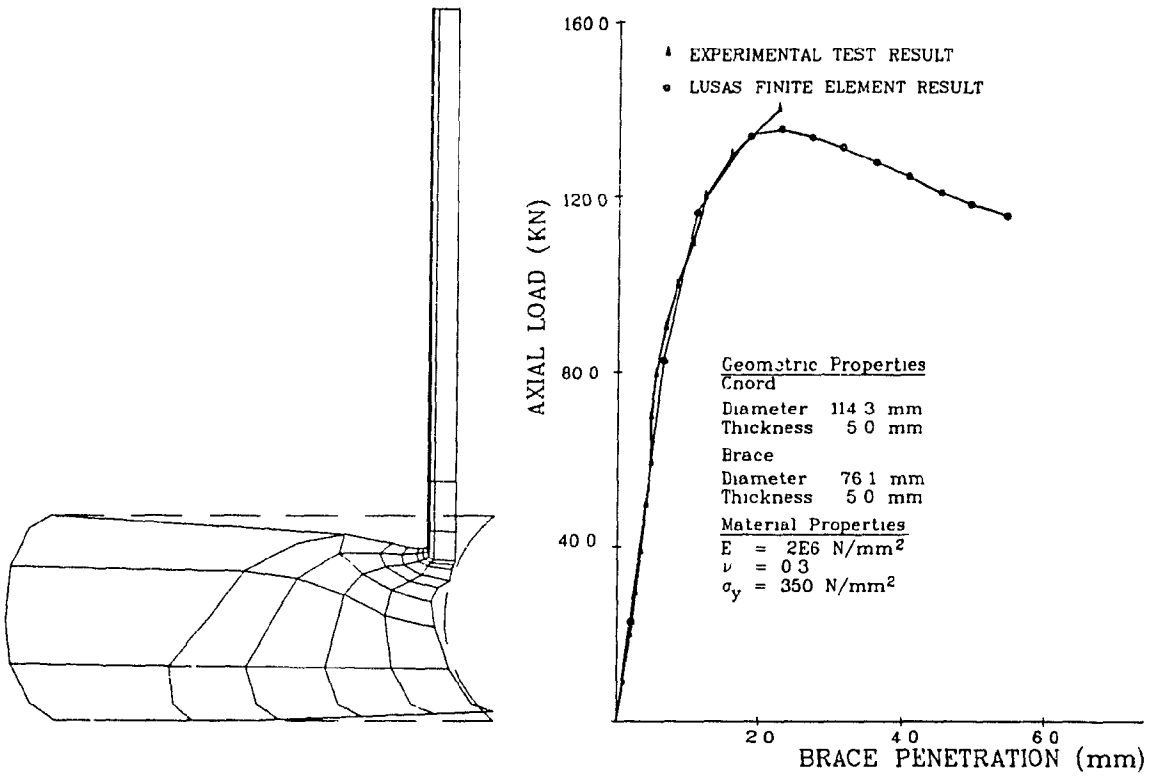

Figure 1.6 Lusas Results[15].

popularity and speed of mini computers the FEM will continue to remain an effective design tool for engineers[15] and to be used in research work alongside laboratory tests.

Three major experimental techniques have been employed to determine stress distribution in tubular joints. They involve testing of

(a) steel models,

(b) acrylic models, and

(c) photoelastic models.

A detailed discussion of various aspects of each of these techniques can be found in the UEG Report[1]. Only a brief sypnosis of some results will be given here.

Strain gauge studies on steel models appeared essential as they provided a database against which other models could be compared. Early studies were carried out at the University of Texas[3,16]. Eleven T-joints were tested, first elastically under a variety of static loading conditions and then under cyclic loading to fatigue failure. Yamasaki, Takizawa, and Komatsu[17] collected strain gauge data from five large T-joints. They concluded that although SCF's were not affected by size effects, fatigue life was. Consequently, they warned about the importance of considering size effects when using data obtained from a small scale test.

Acrylic and photoelastic models, having much lower modulii of elasticity than steel models, are tested using smaller experimental rigs. These models have been popular in Europe since the mid-seventies. The United Kingdom Offshore Steel Research Project (UKOSRP) has undertaken a large research programme to compare the suitability of the different stress-predicting techniques. As part of that research, Irvine, Fessler, and Wordsworth[8] concluded that acrylic and photoelastic models were slightly more accurate than thin shell finite element analysis.

The static strength requirements for tubular joints in the 1960's and 1970's evolved from the punching shear model shown in Fig. 1.7. The nominal punching shear stresses were calculated, multiplied by various correction factors, and compared to the allowable

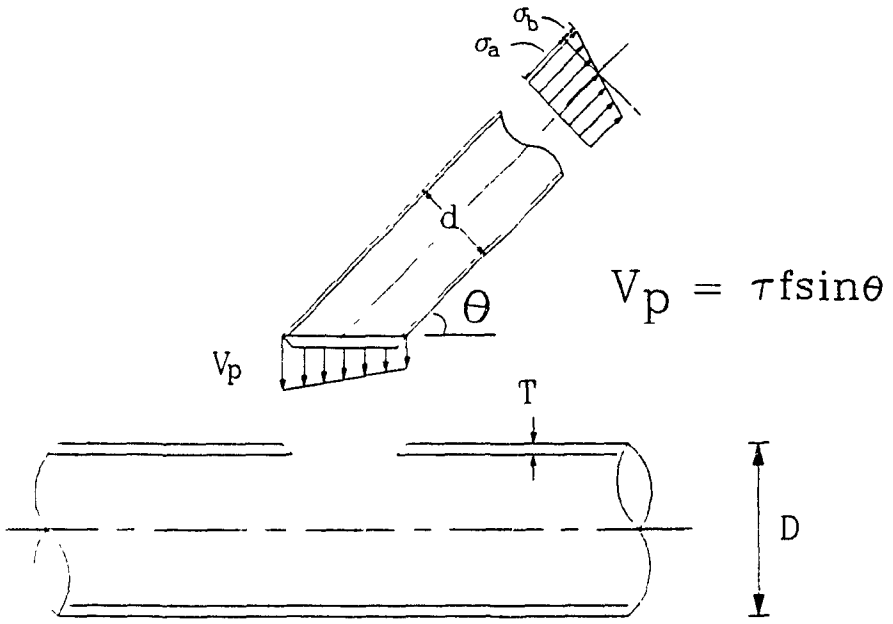

Figure 1.7 Punching Shear Model.

stresses.

As the Limits State Design (LSD) approach has become more widely used more researchers have tested joints to determine their ultimate static strength. By comparing the ultimate load of twelve T- and Y-joints to their hotspot yield load Reber[11] concluded that for T-joints the ratio $[\frac{P_u}{P_y}]$ is 5.8. Yamasaki et al[17] after testing five large diameter connections observed a constant ratio $[\frac{P_u}{P_y}]$ of 4.5. This approach does not seem to have been pursued further.

The design equations which are currently used tend to express the ultimate strength of the joint in terms of a branch axial load. These equations are usually empirical and are obtained by means of statistical analysis of a carefully screened database. With this approach Yura[18] derived the equation shown in Table 1.2. The 1984 API[12] and AWS[19] codes accepted similar, but lower bound equations to the ultimate strength proposed earlier by Yura et al[20]. The allowable branch axial load in these codes was obtained by using a factor of safety of 1.7 and 1.8 respectively. It must be noted that

the API and AWS codes also express their strength requirements in terms of punching shear. Wardenier[21] notes that these equations are no longer based on some modified theoretical shear concept but on the ultimate strength and are intented to be equivalent to the ultimate strength equations just mentioned. Table 1.2 also presents the ultimate strength equation proposed in the UEG Report[1]. This equation was first published by Billington, Lalani, and Tebbett[22] and is based on 45 datapoints which were obtained by the UEG worldwide compilation of reported tests in 1983.

Table 1.2 Strength Equations

Yura[18] 1985	T-joint	$P_u = (3.1 + 20.9\beta)\sigma_y T^2$
(Mean)	DT-joint	$P_u = (2.2 + 17.3\beta)Q_\beta \sigma_y T^2$
Billington et al[22]	T-joint	$P_u = (4.1 + 20.3\beta)Q_\beta \sigma_y T^2$
1983 (Mean)	DT-Joint	$P_u = (3.0 + 15\beta)Q_\beta \sigma_y T^2$
Kurobane et al[26]	T-joint	$P_u = 4.83(1 + 4.94\beta^2)(2\gamma)^{0.233}(\frac{\alpha}{2})^{-0.45}\sigma_y T^2$
1984 (Mean)	DT-Joint	$P_u = \frac{7\ 36}{1-0\ 813\beta}(2\gamma)^{-0.035}\sigma_y T^2$
AWS[19] 1986		$P_u = 18.85 Q_q \beta \sigma_y T^2$
(Lowerbound)		$Q_q = [(\frac{1.7}{\alpha_0} + \frac{0\ 18}{\beta})Q_\beta^{0\ 7(\alpha_0 - 1)}]$
		α_0 = defined in Fig. 1.9
	$Q_\beta = 1$	$\beta \leq 0.6$; $Q_\beta = \frac{0\ 3}{\beta(1-0.833\beta)}$ $\beta > 0.6$

The U. K. Department of Energy and the International Institute of Welding (IIW) use equations based mainly on parameters following from a ring model of the joint (Fig. 1.8). A multiple regression analysis on the available data is then conducted to determine the exponent for each of these parameters Kurobane, Makino, Mitsui, and Ochi[23,24,25,26] have developed and updated the IIW equations as the worldwide

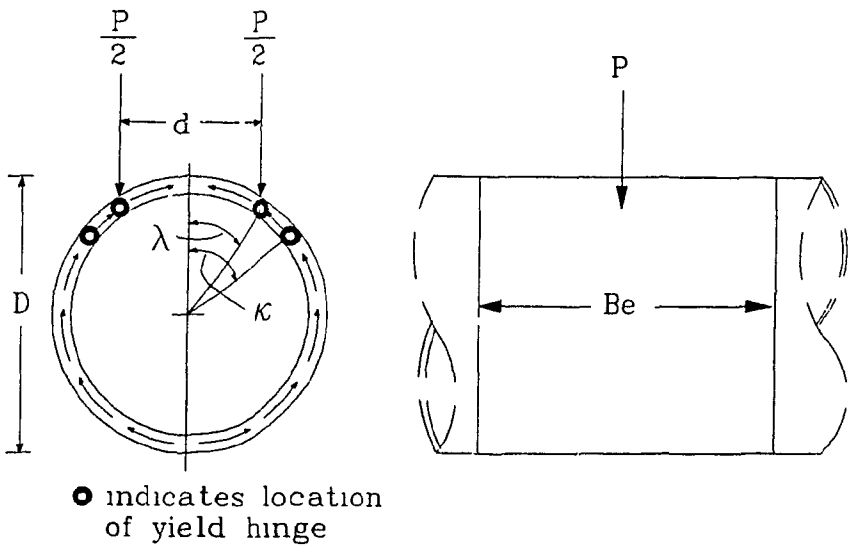

Figure 1.8 Ring Model for T-joint after Kurobane et al[23].

database expanded. Their most recent equation for T-joints is also shown in Table 1.2[26].

As previously mentioned, very little research has been done on V-joints or even on multiplanar joints in general. The next few paragraphs review the information which is currently available.

The UEG[1] reports that strain gauge studies on V-joints have been carried out on steel models by Dijkstra and de Back[27] and by Wordsworth and Smedley[28]. Both series included symmetric tensile loading and antisymmetric loading but neither included symmetric compressive loading. They found that anti-symmetric loading produced higher SCF's and symmetric loading lower SCF's than those from comparable T-joints. Recho and Brozetti[29]carried out a finite element analyses of V-joints. Three of the sixteen joints they modeled were loaded in axial compression. They found that the SCF's were usually lower than for comparable T-joints. They also noted a shift in the hotspot location away from the traditional location at the saddle point. Their results for V-joints in tension compare favourably to experimental results by Dijkstra and de Back[27] and Woodsworth and Smedley[28].

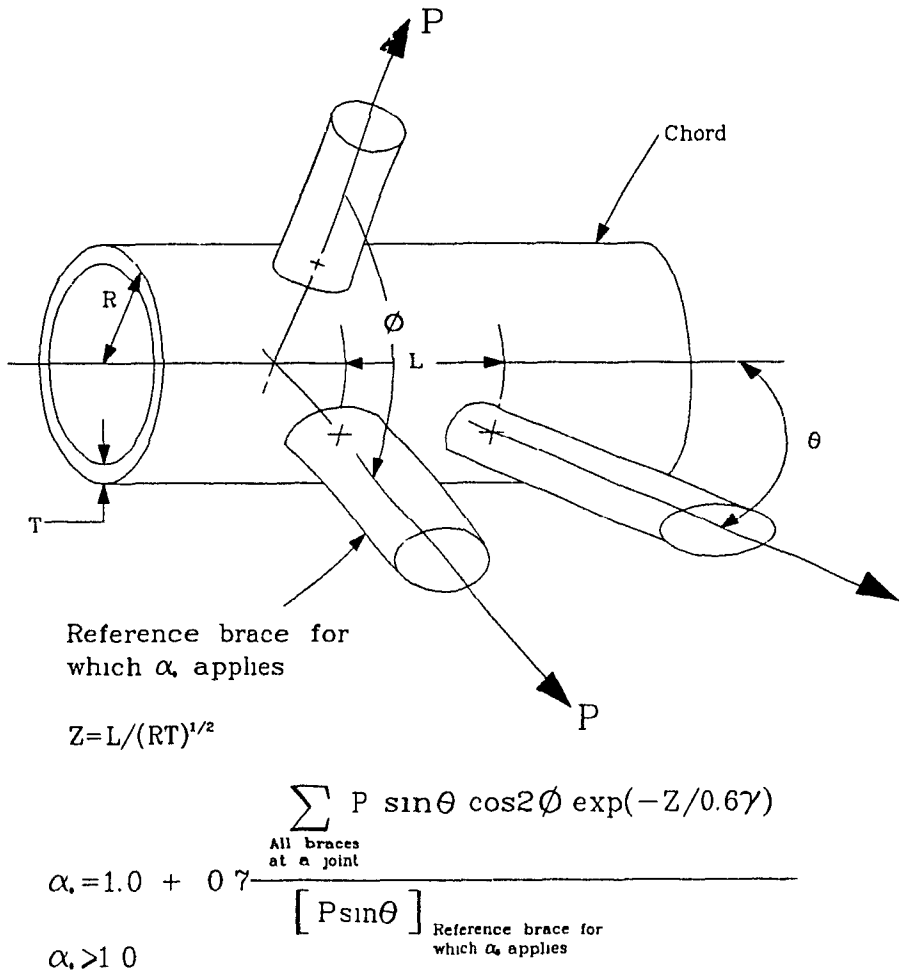

Figure 1.9 Chord Ovalizing Parameter, α_o, as Defined by AWS[19].

The AWS code is the only one to present strength recommendations specifically addressed to multiplanar joints. It is recommended that the load and geometry factor, Q_q, should incorporate a chord ovalizing parameter, α_o, which is defined in Fig. 1.9. Test evidence, like the one presented in this investigation, will help to ascertain the appropriate value of α_0.

1.3 Objectives

The first objective of this research is to establish the first datapoints for a database of V-joints loaded in uniaxial compression. These experimental results are to provide insight on the influences of the various design parameters on the behaviour of V-joints. The experiments should serve to provide direct comparison between the response of V-joints and that of T-joints as both types of connections would be tested as part of this research.

In a second phase it is hoped to develop a simple finite element model for V and T type connections. Shell elements are not to be used but rather program NAF2D[30], which uses beam elements, is to be modified to become TUBE2D, a specialized tubular joint program.

Also, an integral part of this research is to develop pre and post-processors that would enable quick graphical interpretation of TUBE2D input and output. It is of particular interest to create post-processors that would plot the load-deflection curves and the deflected shape of the cross-sections. Such processors along along with the TUBE2D program are to form the TUBE ANALYSIS SYSTEM (TAS), a user-friendly, microcomputer package for design and analysis of tubular V-joints.

CHAPTER 2

EXPERIMENTAL PROGRAM

2.1 Introduction

The scarcity of experimental data on tubular V-joints as reported in Chapter 1 made it imperative that any investigation into the behaviour of axially loaded V-joints include a testing program. The experimental results obtained would not only start a statistical database but also help in the development of analytical models as well as in the verification of their adequacy.

The testing program which was undertaken to study the influence of the different design parameters on the behaviour of V-joints has been partially described in Reference 31 but more complete details are given in this chapter. The program of tests comprised eight V-joint specimens, six T-joint specimens and one DT-joint specimen. The purpose of testing T-joints was to provide a direct comparison with V-joints and also examine the widely used assumption that a V-joint can be treated as two independent simple T-joints.

2.2 Design Parameters

A V-joint with identical branches can be completely described by the following dimensions:

- Chord outside diameter, D
- Branch outside diameter, d
- Chord wall thickness, T
- Branch wall thickness, t
- Included angle between branches, ϕ
- Chord length, L.

In order to facilitate design of tubular joints, the above geometric parameters are normally nondimensionalized by design codes[12,19]. The following notation was recommended in the UEG Report[1] and is used herein:

Diameter ratio,	$\beta = \frac{d}{D}$
Chord thinness ratio,	$\gamma = \frac{D}{2T}$
Wall thickness ratio,	$\tau = \frac{t}{T}$
Chord length parameter,	$\alpha = \frac{2L}{D}$
Out-of-plane angle,	$\phi = \phi$

All of the above dimensions and geometric ratios are identified in Fig. 1.2.

The parameter τ, although influencing elastic stress distribution, has been shown to have little effect on joint strength[1] and was therefore omitted from the current parametric study. Similarly, the ratio α, is also considered of minor consequences (API and AWS do not include it in their strength equation) provided that the chord length and end conditions are chosen so that stress distortions due to end conditions are minimized[32]. The α value for the control joint, T5, in this series of tests, was 4.8, which falls within the parameter range as used in the UEG[1] database for T-joints in compression. Consequently, only the parameters β, γ, ϕ were considered of prime importance to V-joint behaviour and it was their effects which were investigated in this research.

The three geometric ratios chosen were studied using the classical approach to

experimentation where one of the parameters is varied while the other two are kept constant. The parameters were varied within their practical range by assuming three values: a low, middle and a high value. Testing parameters at three levels was considered a minimum to detect the influence of each parameter.

This approach led to a basic experimental matrix of seven V-joints and five T-joints since the parameter ϕ is not applicable for T-joints. A joint with large β was added to this set since ultimate strength is considered highly dependent on β when $\beta > 0.6$[1,4,12]. It should be noted that the large β value could not be introduced with the intermediate value of ϕ since this would have resulted in an overlapping joint. Finally a DT-joint was also added so that extremes of the ϕ series ($\phi = 0°$, $\phi = 180°$) would be tested. All test specimens and their specific parametric values are specified in Table 2.1.

Table 2.1 Experimental Test Program.

Specimen	β	γ	ϕ
V1	0.405	22.90	90°
V2	0.405	13.40	90°
V3	0.645	17.25	90°
V4	0.220	17.25	90°
V5	0.405	17.25	60°
V6	0.405	17.25	120°
V7	0.405	17.25	90°
V8	0.765	17.25	120°
DT1	0.405	17.25	180°
T1	0.405	22.90	
T2	0.405	13.40	
T3	0.645	17.25	
T4	0.220	17.25	
T5	0.405	17.25	
T6	0.765	17.25	

2.3 Specimen Details

All specimens tested had a nominal chord diameter of 219.1 mm. Branch diameters were varied from 48.3 mm to 168.3 mm. The chord sections were cold formed and subsequently stress relieved whereas the branch sections were cold formed to final shape. All chord sections were specified as ASTM A53 GRB steel. Welding was carried out with E70XX (E480XX in S.I.) electrodes and fillet welds were used.

Branch cross sections and weld sizes were selected to ensure that failure would occur by plastic deformation of the chord and not by branch buckling.

2.3.1 Measured Geometric Properties

The chord thickness was measured before testing each specimen using a micrometer. Three readings were made at each end and an average was established. The nominal values of branch thickness were used since their ends were closed. All measured thickness values are reported in Table A.1 whereas averages are shown in Table 2.2.

The chord inner diameter was measured three times at each extremity. Values were recorded and averaged and twice the average thickness was added to obtain outside diameters as shown in Table A.2. The circumference was also measured at each end, averaged and divided by π as shown in Table A.3. The outside diameter obtained by both methods was averaged. Average values are presented in Table 2.2.

The branch circumference was measured near the chord and near the support. The values were averaged and divided by π. Measured values are given in Table A.4 and averages are shown in Table 2.2.

The branch angle ϕ was measured to the nearest degree with a bevel. The vertical angle θ between branch and chord was measured to verify the perpendicularity of the branch. Measured angles ϕ are given in Table 2.2.

Table 2.2 Average Geometric Properties of Experimental Specimens.

Specimen	D (mm)	d (mm)	T (mm)	t (mm)	$\phi(°)$
V1	219.95	89.1	4.92	4.78	90
V2	220.0	89.3	8.24	4.78	90
V3	220.25	142.3	6.315	6.55	90
V4	220.35	49.0	6.34	4.78	90
V5	220.4	89.6	6.39	4.78	60
V6	219.9	89.3	6.39	4.78	120
V7	220.5	89.8	6.32	4.78	90
V8	220.25	169.3	6.30	4.78	120
DT1	220.2	89.3	6.30	4.78	180
T1	219.85	89.0	4.94	4.78	
T2	219.95	89.3	8.21	4.78	
T3	220.0	141.8	6.40	6.55	
T4	220.25	48.7	6.37	4.78	
T5	219.6	89.0	6.39	4.78	
T6	220.4	169.0	6.38	4.78	

2.3.2 Material Properties

Two steel coupons were tested in accordance with the American Society for Testing Materials (ASTM) standards[33] for each of the three chord thickness. The stress-strain curves were plotted and the 0.2% strain offset method was used to determine the yield strength. The familiar bi-linear idealization was then used to determine Young's and Tangent Modulus. Percent elongation was also determined. Measured material properties together with ASTM specifications are given in Table 2.3.

In addition to the standard coupon tests, two stub column tests were performed for each thickness of chord section. All dimensions, slenderness ratios and testing procedures were in accordance with the Column Research Council Technical memorandum[34]. The instrumentation consisted of 4 strain gauges located at mid-height, each 90° apart

and three LVDTs, each 120° apart. Stress-strain curves were plotted and the material properties obtained are shown in Table 2.4. A complete set of stress-strain curves for chord 219.1 × 6.35 is given in Appendix B. The steel coupon properties are used in the rest of this report.

Table 2.3 Steel Coupon Properties.

Chord Section	219.1 ×4.78	219.1 ×6.35	219.1 ×8.18	ASTM A53 GRB
Yield Strength (MPa)	335	327	400	240
Ultimate Strength (MPa)	465	458	482	415
% Elongation	32	35	23	19.5, 20, 21.7
Young's Modulus (MPa)	190000	196000	208000	
Tangent Modulus (MPa)	2500	1800	2750	

Table 2.4 Stub Column Properties.

Chord Section	219.1 ×4.78	219.1 ×6.35	219.1 ×8.18	ASTM A53 GRB
Yield Strength (MPa)	325	338	376	240
Ultimate Strength (MPa)	377	397	460	415
Young's Modulus (MPa)	192000	191000	204000	
Tangent Modulus (MPa)	4200	3300	4800	

2.4 Instrumentation

This section describes in detail the instrumentation used to monitor the response of the specimens. Instrumentation consisted of LVDTs (Linearly Variable Differential Transformers) and 5 mm electric wire resistance strain gauges. LVDT and strain gauge

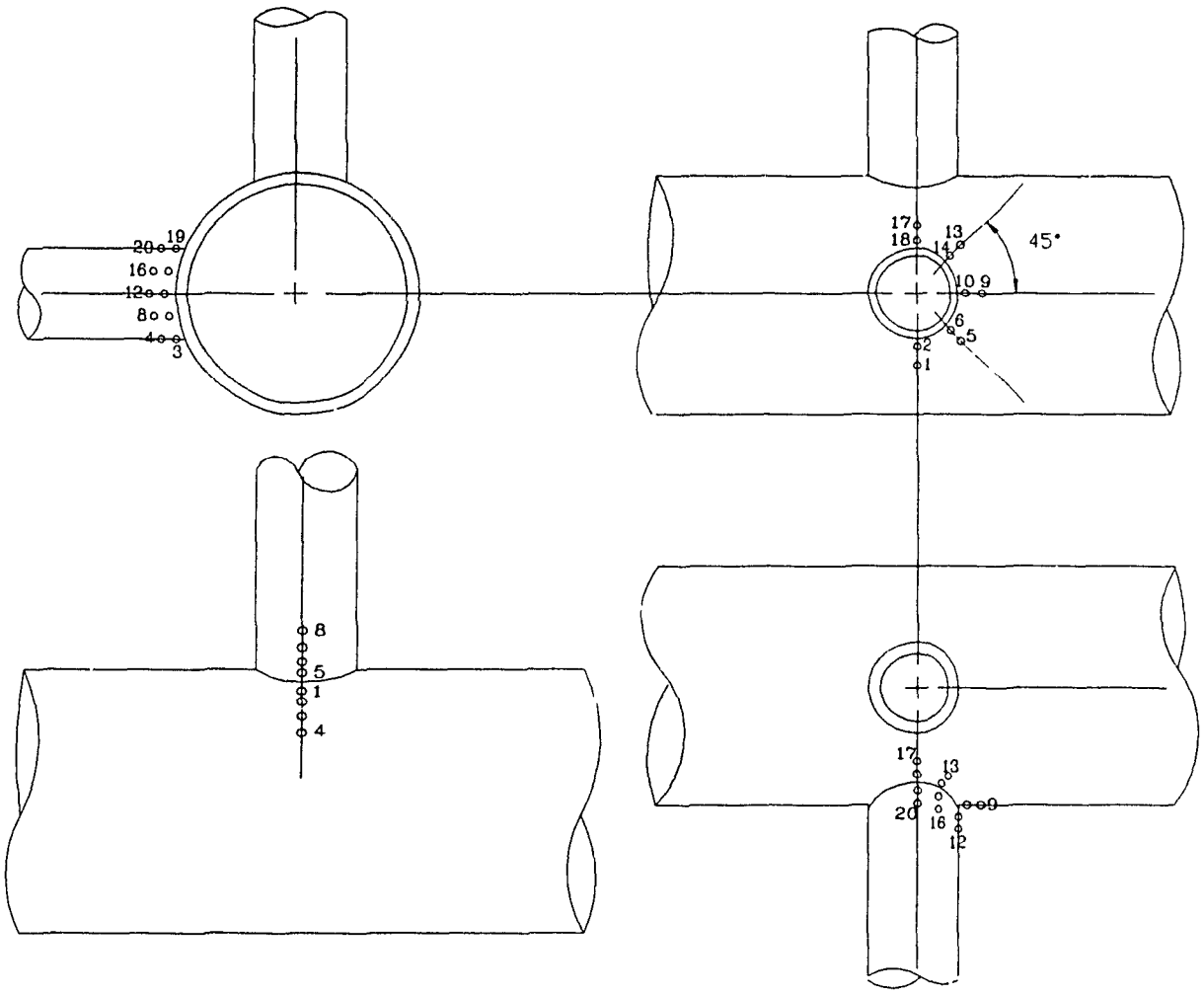

Figure 2.1 Strain Gauge Location.

readings were collected through an Optilog multi-channel recorder and sent to an Apple IIc Computer which stored the data on diskettes. Details of the measurements taken are given below.

2.4.1 Strain Gauges

The location of strain gauges for T and V-joints are shown in Fig. 2.1.

Only one line of gauges was used for T-joints since the hotspot is known to be located at the saddle of the branch chord intersection[1,4]. The location of the four gauges closest to the weld were calculated in accordance with the United Kingdom Offshore

Steel Research Project recommendations for defining stress concentration factor at the weld toe which are presented in Fig. 2.2. Often the calculated spacing was smaller than the physical length of a gauge in which case the two gauges were placed as close as possible to each other. The additional four gauges were used to obtain a more complete stress profile.

Where possible, five lines of four gauges were placed on each V-joint. The gauge spacing was in accordance with UKOSRP recommendations and radiated from the branch. The lines were spaced at 45° around the branch beginning at the back of the joint and ending at the crotch. In specimens with either high β ratio (V3) or low ϕ (V5) the lack of chord space between the branches prevented placement of gauges on the chord at the crotch.

2.4.2 LVDTs

LVDTs were used to measure both branch penetration into the chord as well as the chord deflection in the longitudinal direction.

For T-joints the branch penetration was measured by attaching two LVDTs to the side of the branch and measuring deflections with respect to a thin plate attached to the back of the joint as shown in Fig. 2.3(a).

To obtain the branch penetration into the V-joint chord small frames were tack welded to the back of the joint to hold the LVDTs in axial alignment with the branches (Fig. 2.3(b)). Each LVDT core was attached to a thin rod which reached inside the chord, through a 3 mm drilled hole, to the geometric center of the branch. The tip of the thin rod was prevented from slipping during the testing by glueing it to the branch with a small amount of silicone caulking.

Four LVDTs were used in both T and V-joints to record beam action and overall settlement. At first these LVDTs were mounted on the specimens but unsatisfactory results required that they be placed on frames resting on the test floor. The T-joint

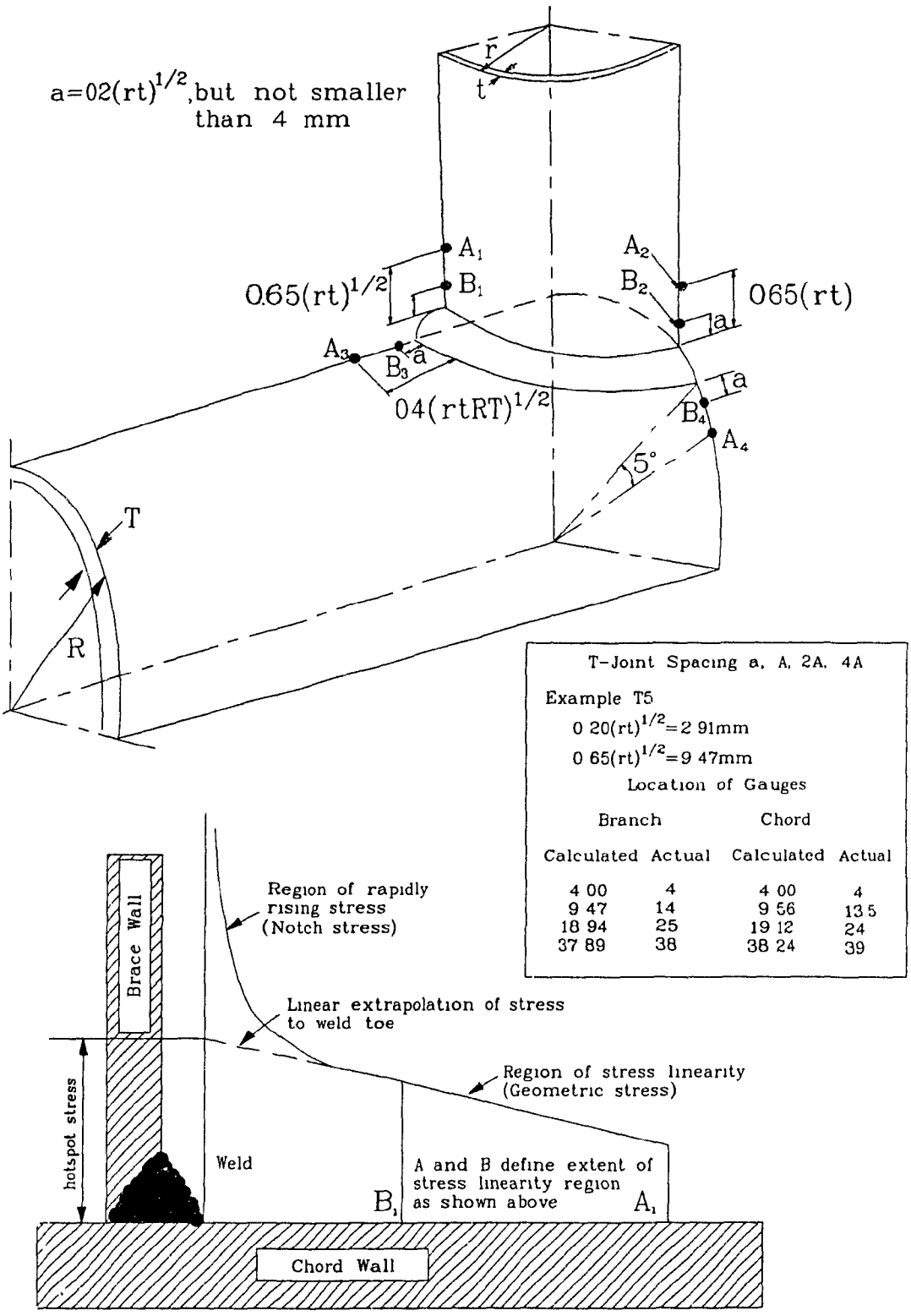

Figure 2.2 UKOSRP Recommended Strain Gauge Spacing for Determining Stress Concentration Factors[1].

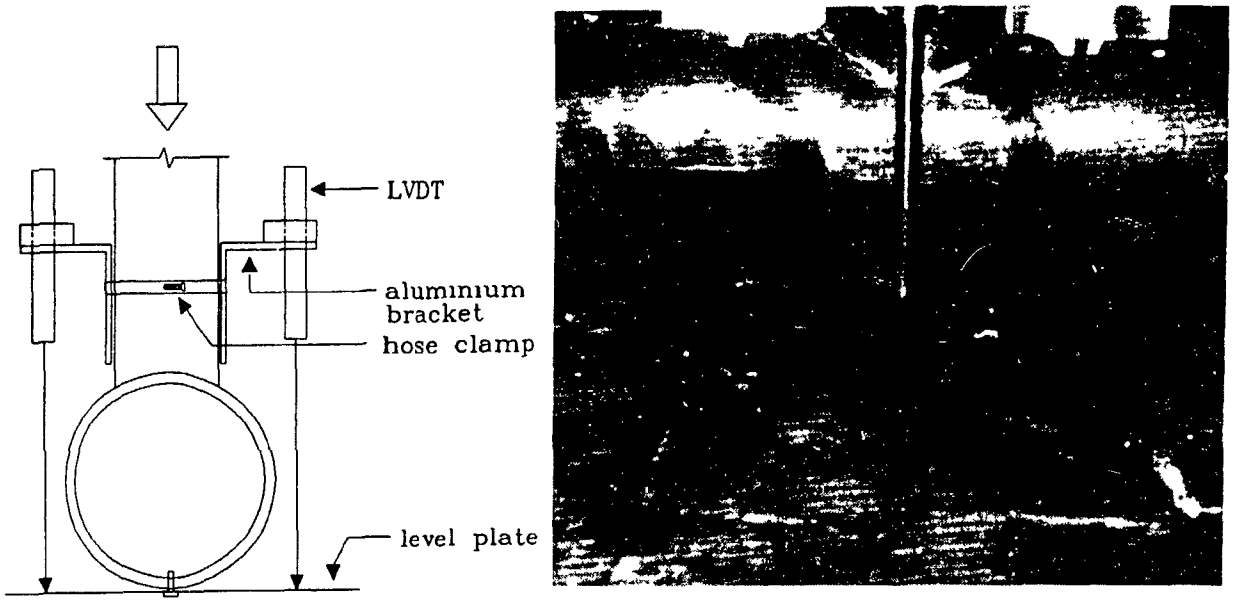

(a) T-joint Branch Penetration

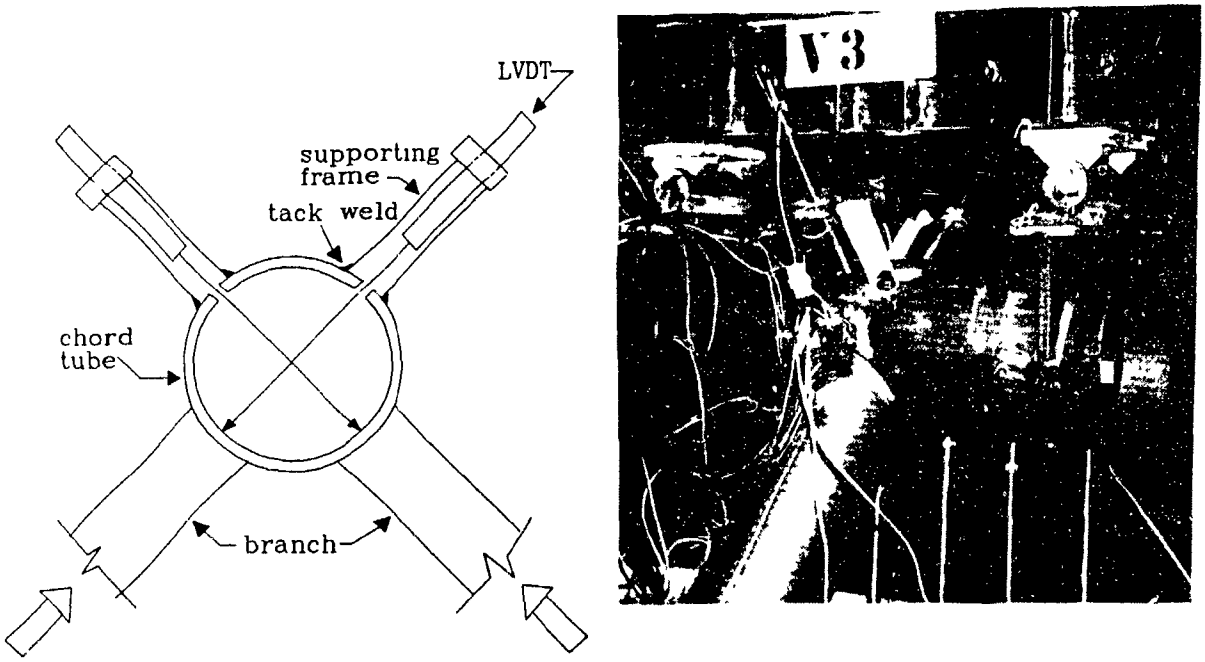

(b) V-joint Branch Penetration

Figure 2.3 LVDT Set-Up for Measurement of Branch Penetration.

LVDTs were placed on the chord crown line as shown in Fig. 2.4(a). The LVDT at the welded toe rested on a small angle glued to the branch to measure the precise chord deflection at the branch chord intersection. The spacing of the LVDTs on the V-joints corresponded to those of the T-joints but the profile taken was that of the crotch line (Fig. 2.4(b)).

2.5 Test Arrangement

A sketch of a V-joint specimen in its test position is shown in Fig. 2.5a. Figures 2.5b and 2.5c show a specimen with full instrumentation, ready to be tested. Two sets of back to back stiffened channels were used to provide headroom under the universal testing machine for the LVDTs used to measure branch penetration. Hinge supports, formed by welding a machined cylinder to a plate and resting the cylinder in its semi-circular receptacle, then transfer the load to the chord member through two loading caps. These caps were spaced at a distance $2D + d$ and shimmed to ensure complete contact. Furthermore the chord was reinforced at the loading points by diaphragms to prevent its distortion at these sections.

The branches rested on knife-edge supports. Short base supports of differing angles were fitted to the specimen and were connected to a base beam which rested on a strong floor. The base beam was laterally braced to the testing machine (Fig. 2.5b).

The T-joint set-up was simpler. The joint was tested in an inverted position. Vertical compression was applied to the branch through a ball bearing joint while the chord was supported by two knife-edge supports placed on the strong floor as shown in Fig. 2.6. The T-joints were reinforced at the loading points in the same fashion as the V-joints.

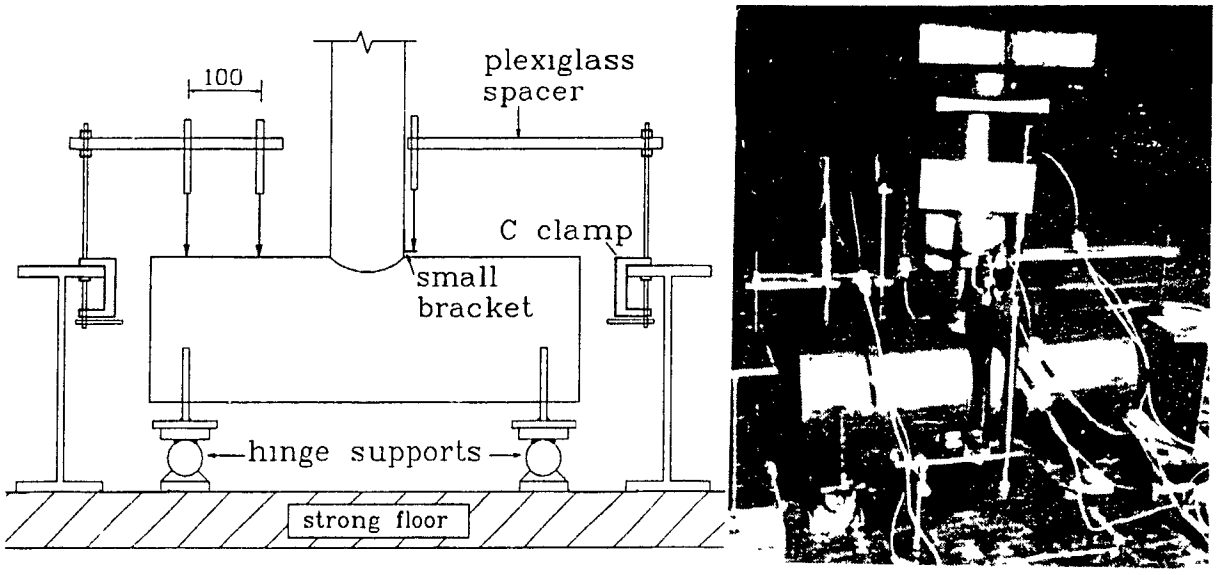

(a) T-joint Crown Line Profile

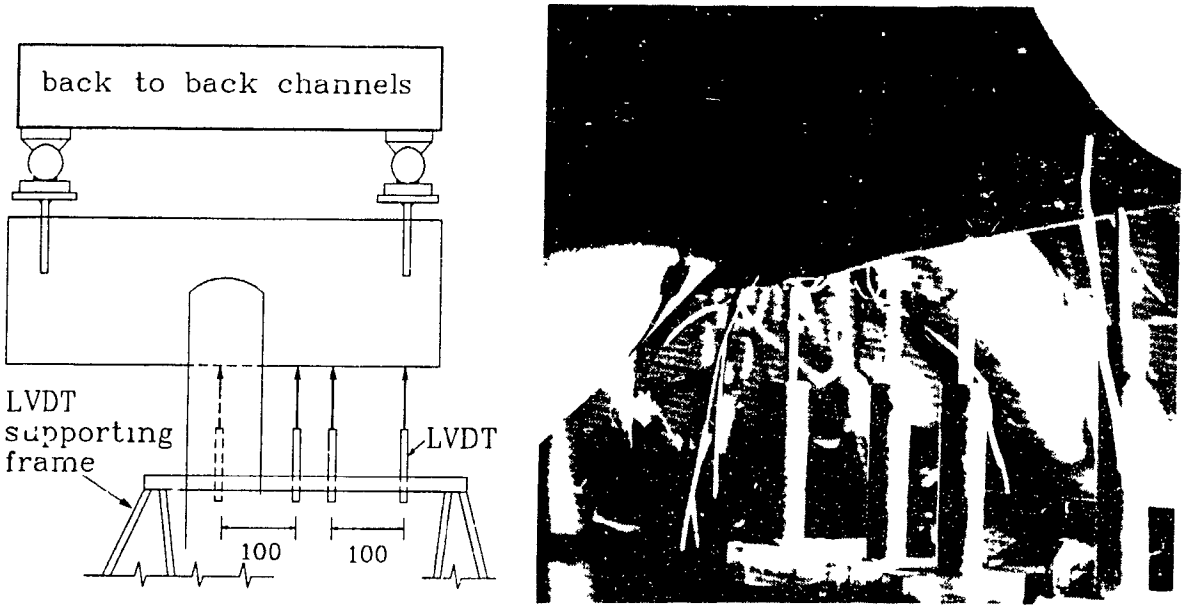

(b) V-joint Crotch Line Profile

Figure 2.4 LVDT Set-Up for Measurement of Chord Profile.

2.6 Testing Procedure

All loads were applied vertically downwards by a 2000 kN universal testing machine. The loads were recorded to the nearest 0.5 kN using the load cell integral with

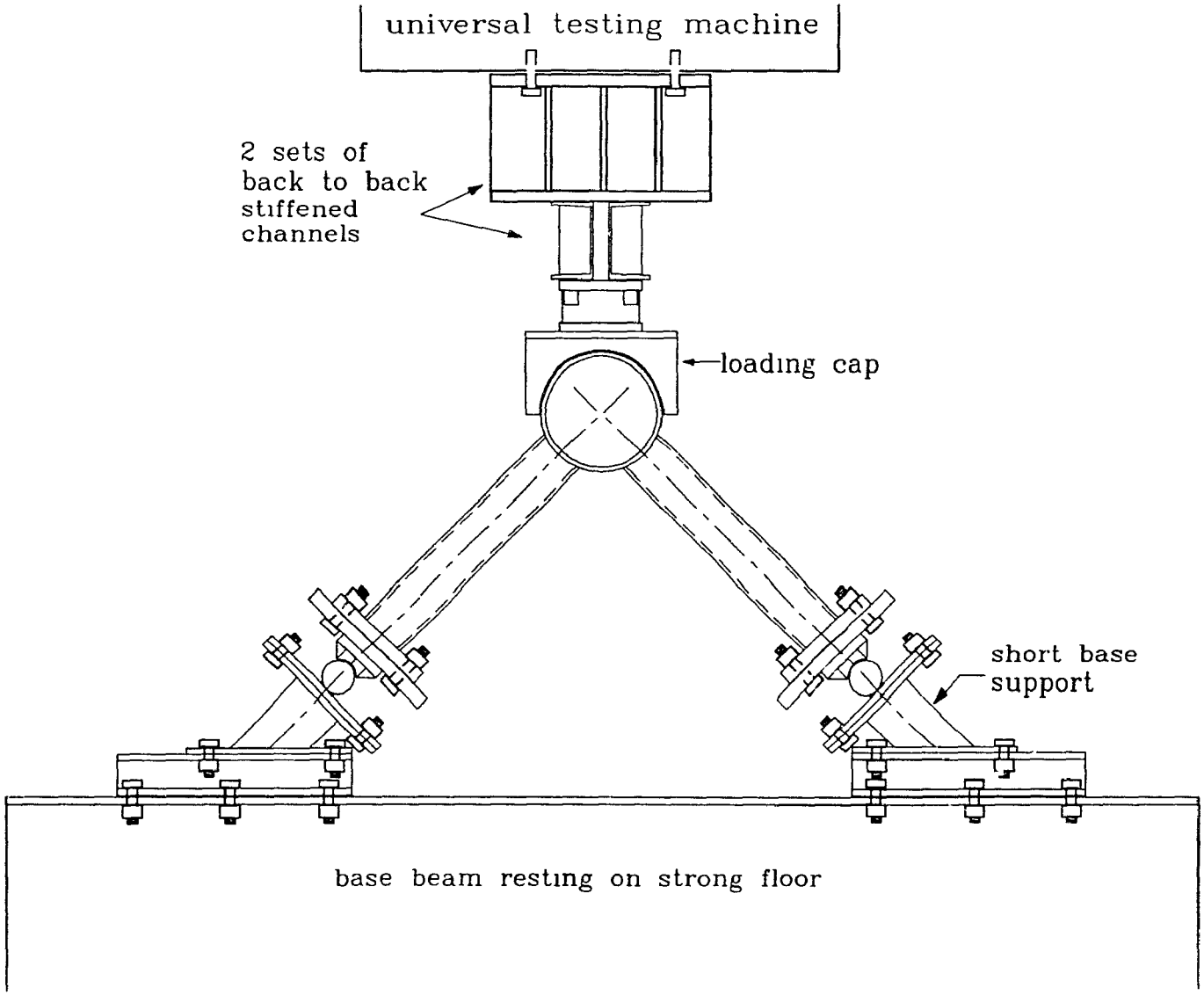

(a) Details of Loading Arrangement

Figure 2.5 V-joint in Testing Position.

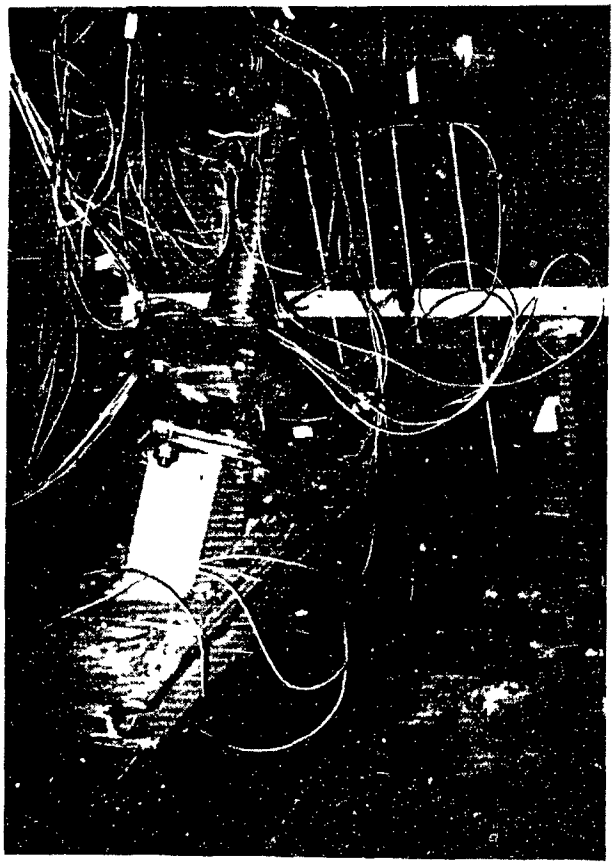

(b) Short Base Support, Base Beam, and Lateral Bracing

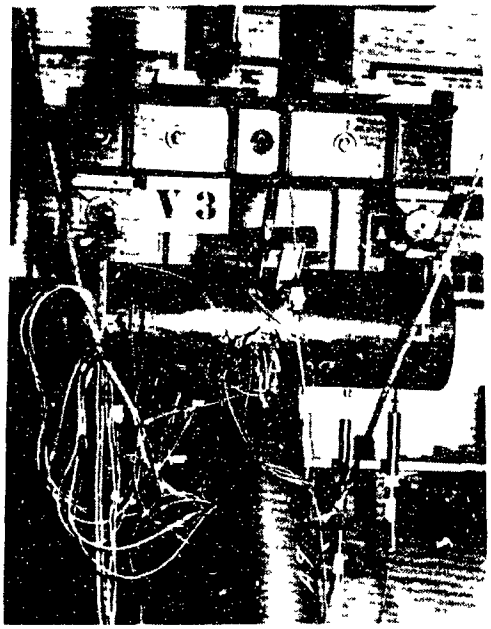

(c) Stiffened Channels, Loading Hinges, and Loading Caps

Figure 2.5 V-joint in Testing Position (Continue).

the testing machine.

A load of approximately 2 kN was applied before testing to settle in the specimen and obtain initial readings. Load increments of 10 to 25 kN were then applied quasi-statically. The magnitude of the increments was dependent on the expected ultimate strength and selected to be small enough to reflect the nonlinearity of the response but sufficiently large to limit each test to between 20 and 50 load increments. At the end of each increment, the load was held constant while the deflections and the strains were recorded.

Smaller increments were applied as the joint stiffness was reduced and the load

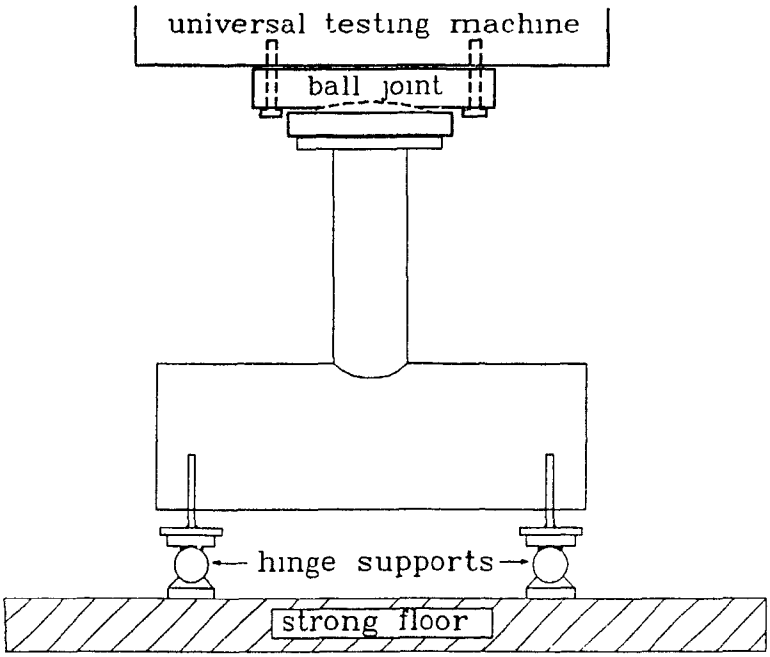

(a) Loading Arrangement

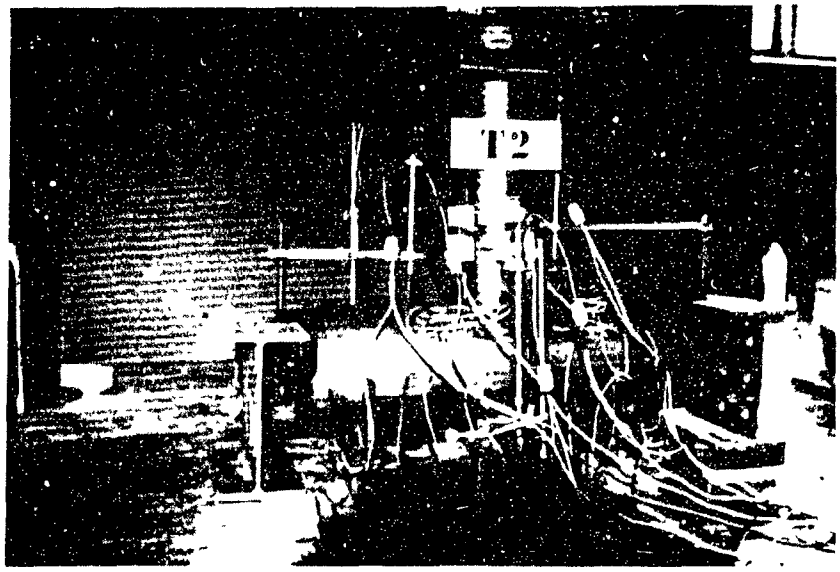

(b) Specimen T2 Ready to be Tested

Figure 2.6 T-joint in Testing Position.

approached its ultimate value. Attempts were made to record data past the point of peak load.

2.7 Test Results

The measurements of load, strain and displacement taken during testing of a joint were used to examine each specimen's behaviour from four different perspectives:

(1) ultimate strength

(2) load vs. branch penetration

(3) stress concentration factors

(4) profile deformation.

These cases are discussed below in the following subsections.

2.7.1 Ultimate Strength

The peak load was recorded in each test. For T-joints the peak load is entered directly as the joint ultimate strength. For V-joints, on other hand, the downward load is resolved into two equal branch axial forces, the maximum magnitude of which is recorded as the joint ultimate strength. Results are presented in Table 2.5. Also shown in Table 2.5 are the ultimate strengths of the joints as predicted by the formulae proposed by Ochi, Makino and Kurobane et al[26], Yura[18], the AWS[19] code, and the UEG[1]. The T-joint formulae were also used to estimate the V-joint strength in all cases except for the AWS code which proposed a formula that can be specifically applied to V-joints. The ultimate strength of DT1 is estimated with both T-joint and cross-joint formulae given in References 1, 18, and 26.

As can been readily seem from Fig. 2.7, best agreement appears to be Kurobane et al's formula, while Yura's, the UEG's , and the AWS's predictions were always below T-joint experimental ultimate strength. Not surprisingly, AWS values are consistently the lowest as they are based on earlier lower bound ultimate strength formula provided

Table 2.5 Ultimate Strength Predictions and Experimental Results.

Joint	Billington	Kurobane	Yura	AWS	AWS μ	Test	Test μ
V1	99.0	115.8	93.8	132.8	1.48	131.5	1.14
V2	335.1	344.7	314.6	445.5	1.48	383.7	1.16
V3	225.7	284.6	216.4	314.2	1.54	452.9	1.38
V4	113.1	125.9	101.7	138.1	1.38	122.0	1.00
V5	164.9	180.0	154.8	174.1	1.18	238.8	1.14
V6	164.7	179.8	154.7	173.9	1.18	177.4	0.85
V7	161.4	176.7	151.6	214.7	1.48	206.3	0.99
V8	277.6	355.7	248.8	286.6	1.18	458.1	1.20
$DT1_+$	117.9	125.8	119.6	114.3	0.80	157.4	0.75
$DT1_T$	160.0	175.2	150.2	143.2		157.4	
T1	100.7	116.6	94.5	90.1		115.2	
T2	332.7	342.4	312.3	297.8		330.5	
T3	231.3	290.5	221.9	208.7		328.7	
T4	113.9	126.8	102.4	100.3		122.3	
T5	164.5	179.3	154.4	147.2		208.6	
T6	283.6	362.5	254.6	247.0		382.9	

by Yura, Zettlemoyer and Edwards[20]. Differences between the remaining three mean strength equations can be attributed to both differences in database screening standards and ultimate strength definition. Kurobane, for example, includes in his database many test results which Yura and the UEG screened out because of size effects (the chord diameters were less than 125 mm). Furthermore, Yura includes a deflection limit in his definition of ultimate load.

Seven out of eight V-joints sustained as much, or more axial load than their corresponding T-joints. This can be expressed as the V-joint strength to T-joint strength ratio, μ, being equal to or greater than one for seven out of eight joints as can be seen in Table 2.5 The influence of ϕ is readily noted from Table 2.5 as V6 ($\phi = 120°$) and

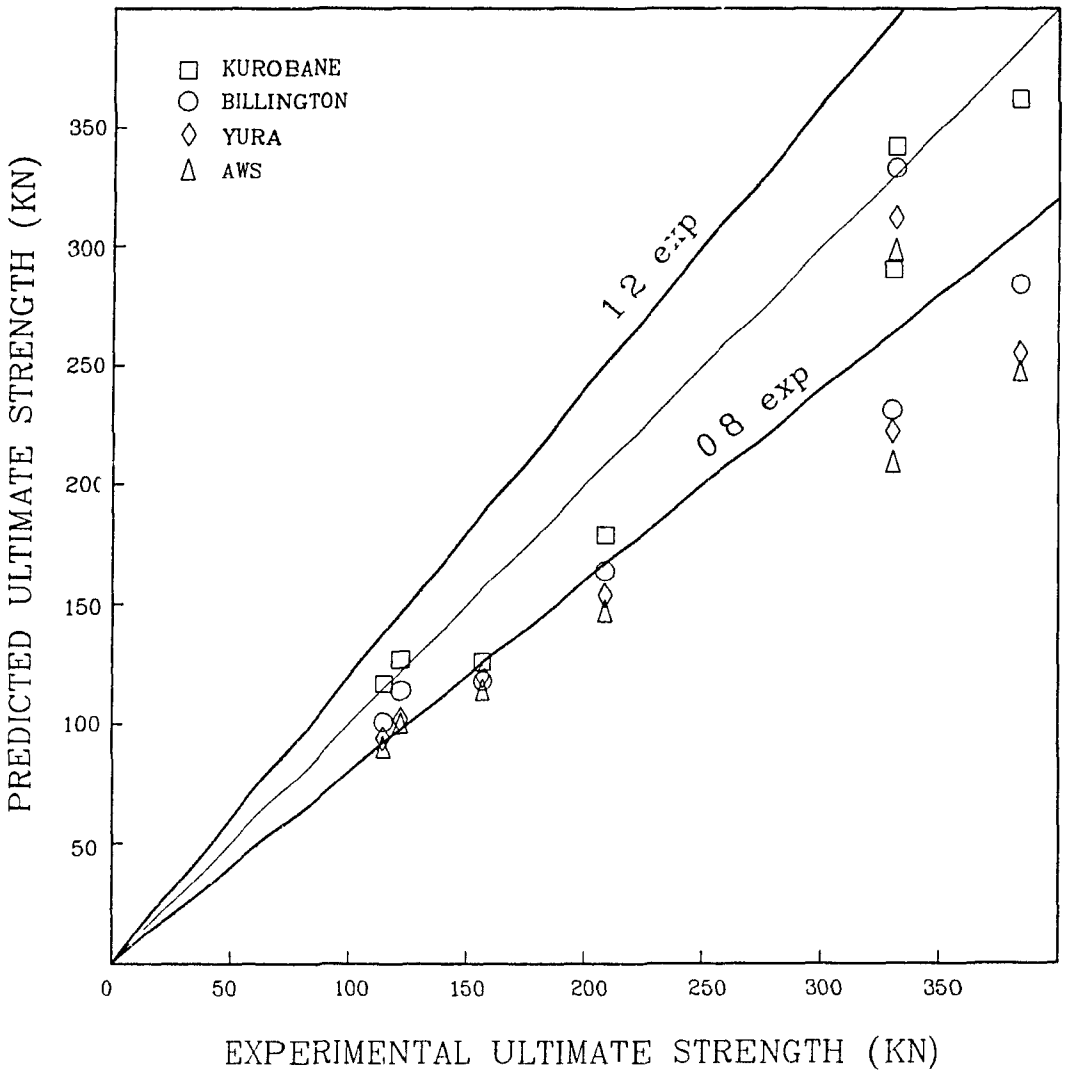

Figure 2.7 Comparison of T-joint Strength Predictions and Experimental Results.

DT1 ($\phi = 180°$) are the only joints weaker than their comparable tee. This reduction in strength as ϕ increases above 90° may be attributed to the tendency of both branches to ovalize the chord in the same sense. On the other hand, when ϕ was less than 90°, V5 ($\phi = 60°$), the ultimate strength was increased. This appears to reflect a tendency of two branches to act as one and hence of the joint to behave as a T-joint with a large β. This tendency is clearly demonstrated in the centerline post-failure cross-sections shown in Fig. 2.8. V5 and T3 show similar cross-sections while V6 shows a different

different mode of collapse. The increased strength for V-joints predicted by the AWS formula was always greater than observed experimentally. Of particular concern are the $\phi = 120°$ results where decreased strength was recorded.

The influence of β is also significant. For small values of β (V4) each branch tends to act independently and hence carry the same load as the branch in a T-joint. On the other hand, Joint V3 with its high β value sustained nearly 40% more load than the corresponding T3. Joint V8, having the highest β could be expected to carry 50 or 60% more than joint T6 but the high angle ϕ between the branches partially counteracted the β effect and reduced the gain in strength to 20%.

Finally the effect of the γ ratio is easily noted and quite understandable. Increasing the γ ratio decreased the ultimate capacity. No trend was detected for the ratio μ as γ was varied, as both high and low γ joints exhibited similar μ values of approximately 1.15.

2.7.2 Load vs. Branch Penetration

Load vs. branch penetration curves are plotted in Figs. 2.9 to 2.11. With the exception of V3, the deformation given represents the average of the two LVDT readings for branch axial penetration. Axial deformations of V8 and DT1 were not taken due to geometric constraints imposed by the specimens. Loads are normalized by dividing by $F_y T^2$ except when the effect of γ is examined because the inclusion of T in the normalizing factor would mask the effect of γ since this parameter is itself dependent on T. Therefore $F_y t^2$ was used as a normalizing factor for the γ series of test results.

It can easily be seen that V-joints are stiffer than similar T-joints. Most V-joints reached ultimate load with less than 2 mm penetration whereas T-joint resistance typically peaked after 5 to 6 mm branch penetration.

Increasing the chord thickness resulted in increased strength and stiffness for both T and V-joints as shown in Fig. 2.9. Similarly, increasing the β ratio increased the

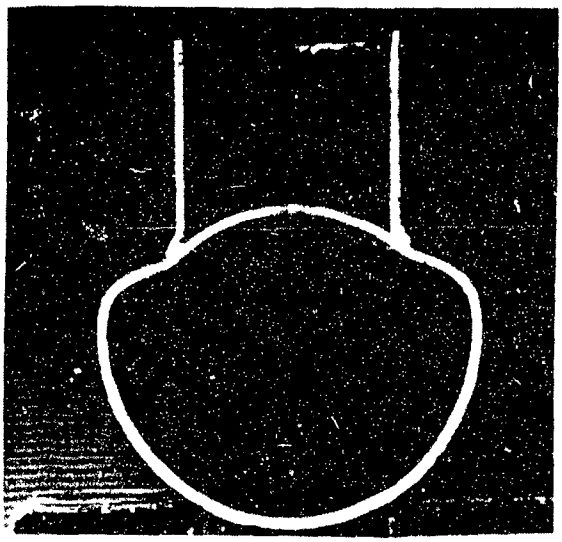

(a) T5

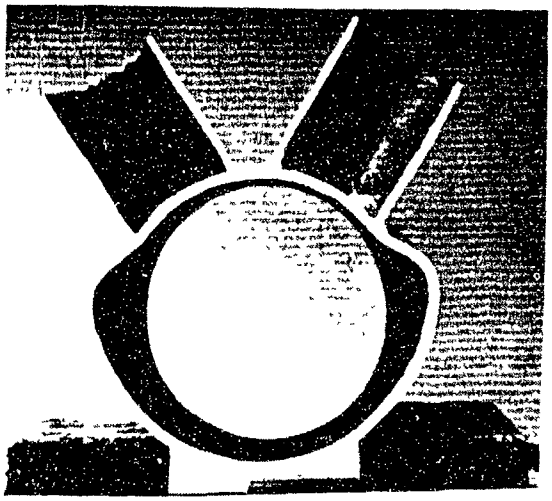

(b) V5

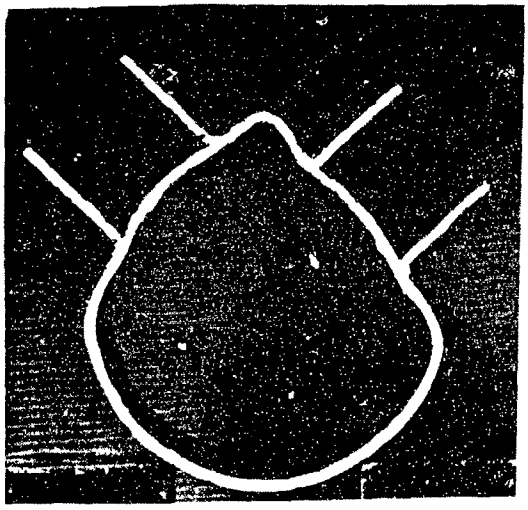

(c) V7

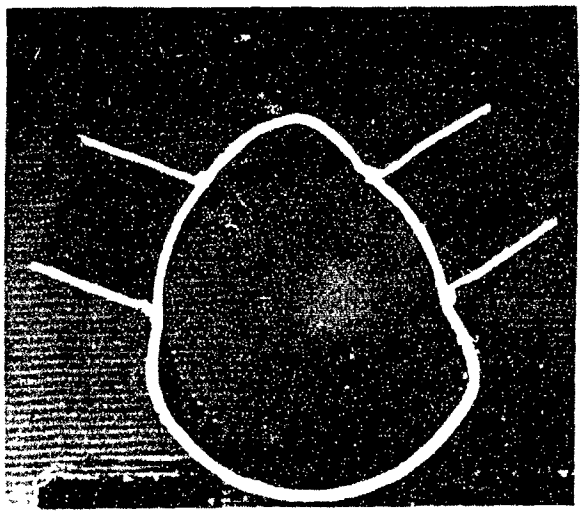

(d) V6

Figure 2.8 Post-Collapse Cross Sections.

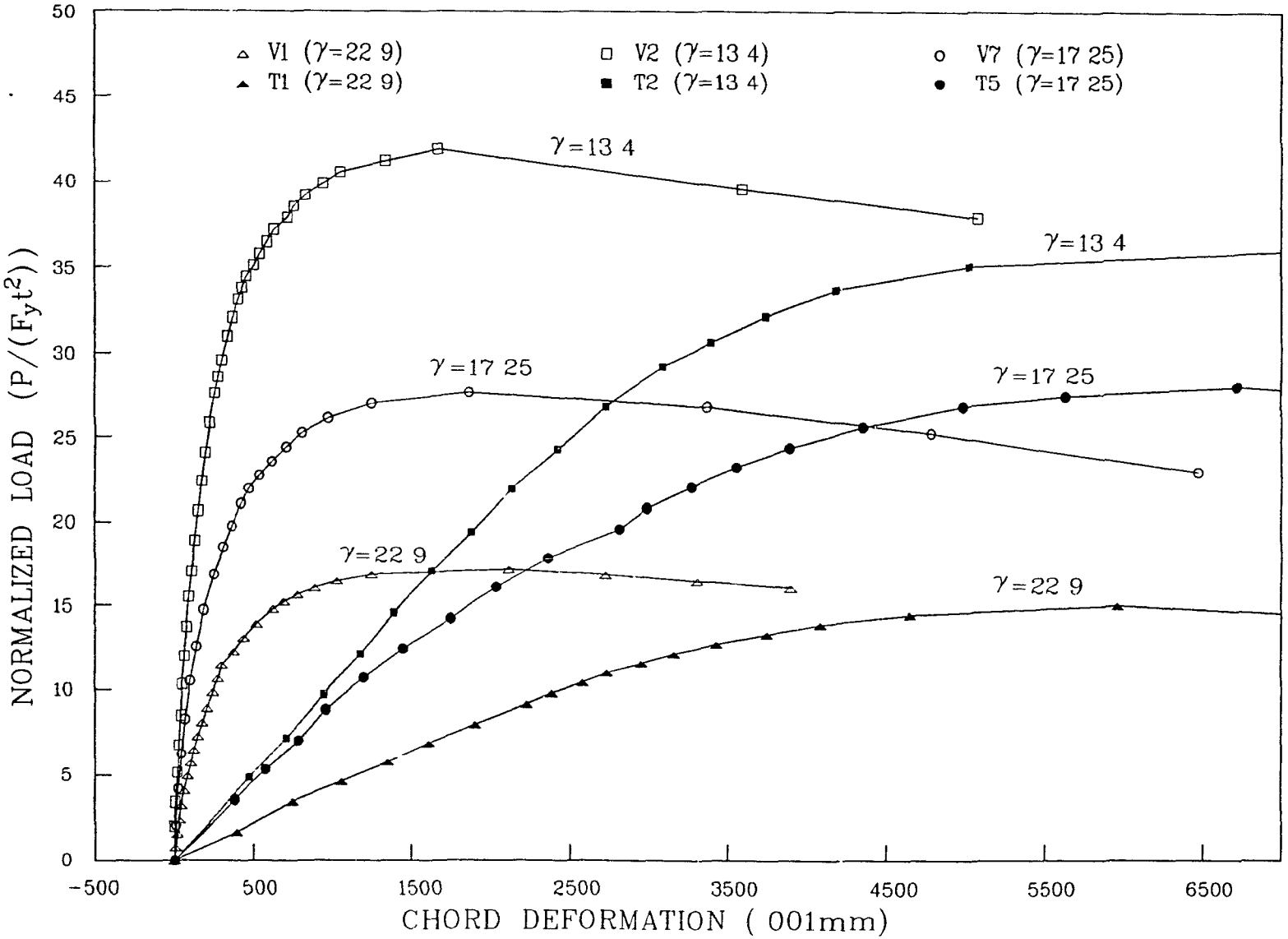

Figure 2.9 Effect of γ on Experimental Load-Deflection Response.

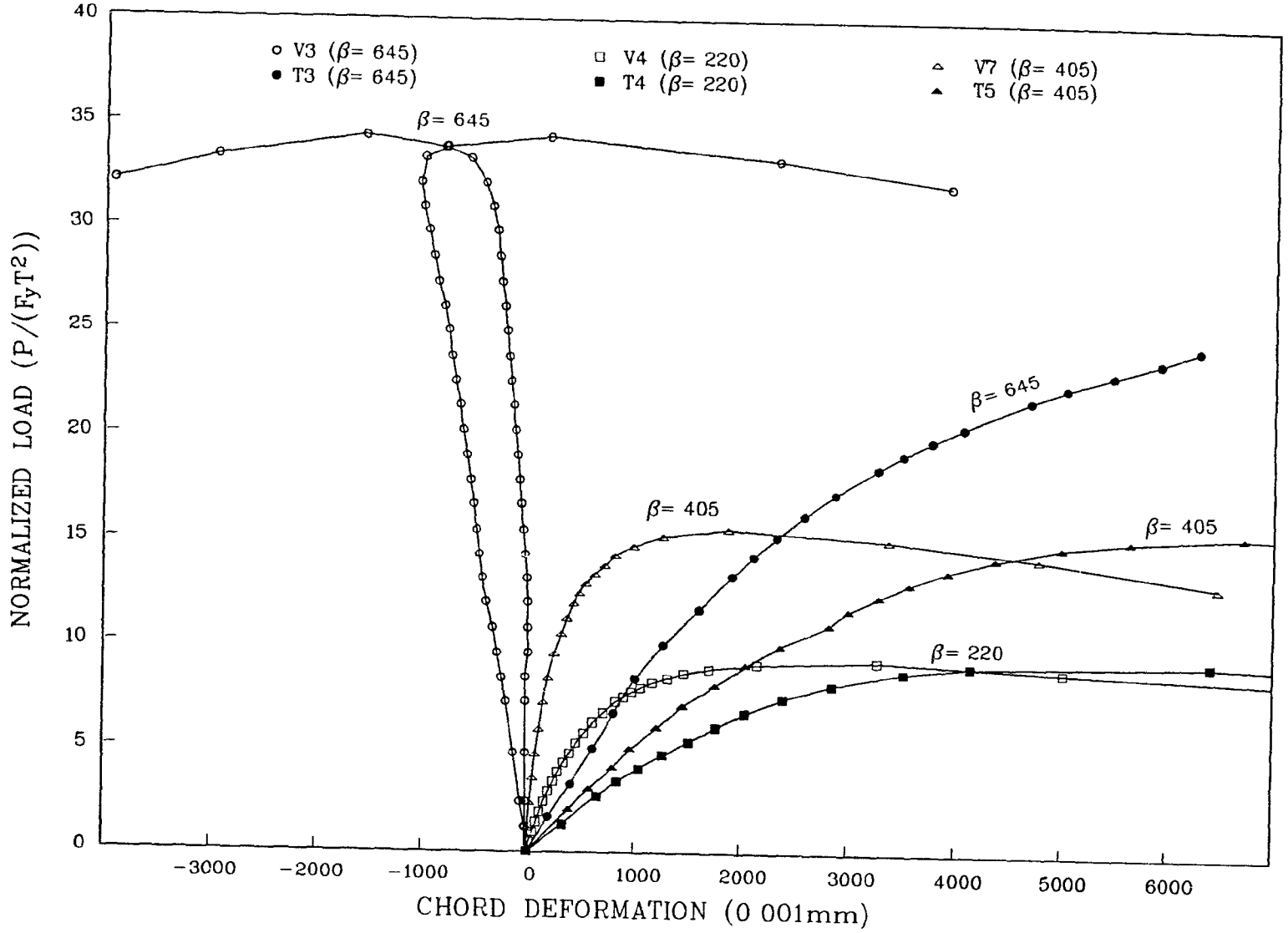

Figure 2.10 Effect of β on Experimental Load-Deflection Response.

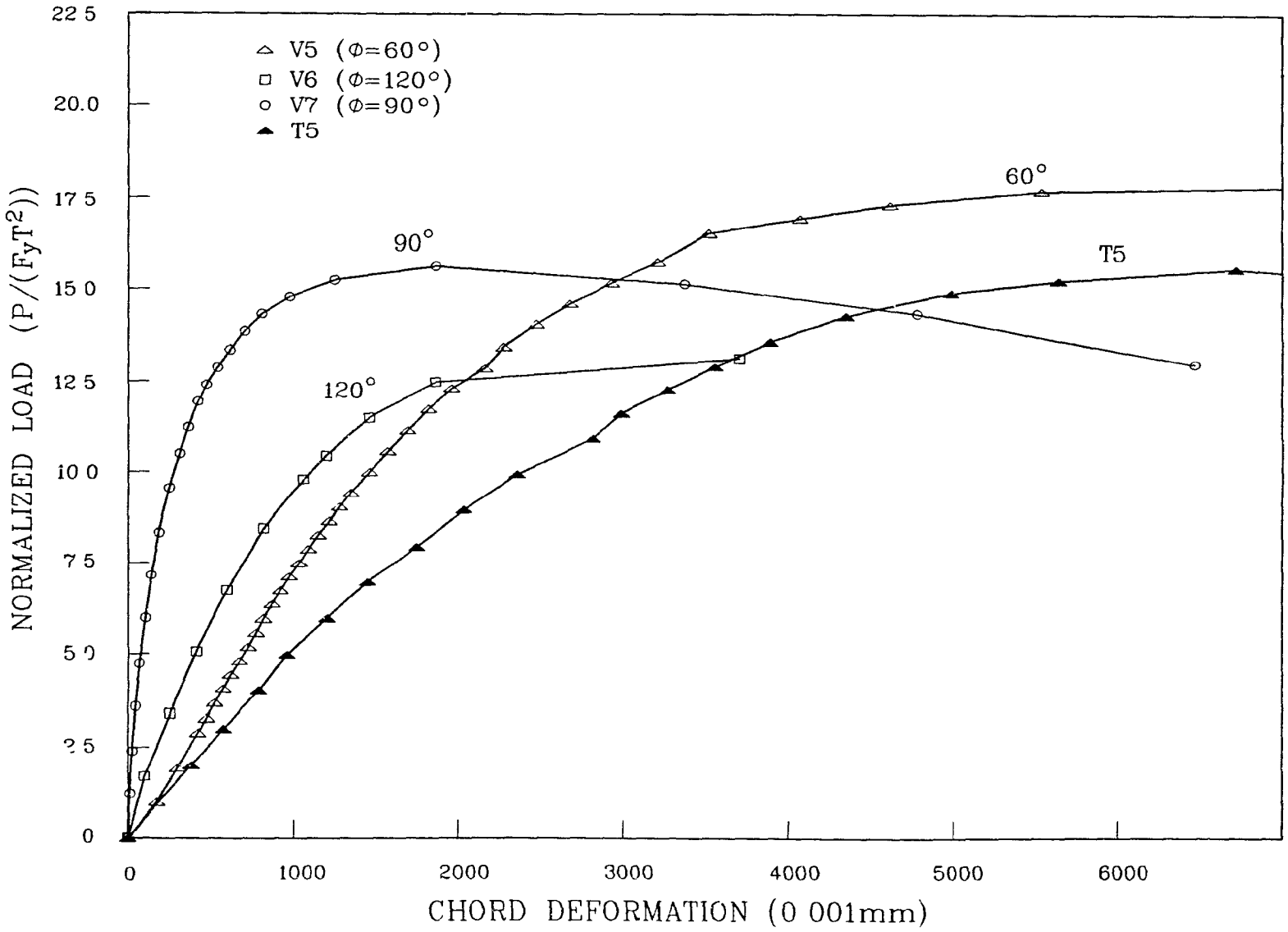

Figure 2.11 Effect of ϕ on Experimental Load-Deflection Response.

strength and stiffness of both types of joint. It was noted, however, that the increases were more substantial for V specimens than for T specimens as V3 carried 3.7 times more load than V4, while T3 carried only 2.7 times more than T4. It is interesting to note that the large branches of V3 did not penetrate the chord but rather ovalized it in such a way that the measured diameters lengthen and therefore negative penetration i.e. axial elongation, was recorded (Fig. 2.10).

Figure 2.11 shows the impact of the angle ϕ on the response of the joint. There appears to be an optimization of stiffness at ϕ near 90° as joints with ϕ either greater or smaller than 90°were more flexible than the 90° angle joint. Strength is not maximized in the same way: although it carried more load than V6 (120°), V7 (90°), sustained less load than V5(60°). With its higher flexiblility and ultimate load joint V5 exhibited a response quite similar to that of T-joints with high β values.

2.7.3 Stress Concentration Factors

Experimental stress concentration factors were determined in accordance with the UKOSRP[1] (Fig. 2.2) and are presented in Tables 2.6 and 2.7. SCFs were calculated for all load levels under 15% of the ultimate load and the highest values were retained. The peak values were typically recorded at the lowest load level and slowly decreased with increasing loads. This behaviour provides a good indication of the shortness of the linear elastic range of the specimens response. Tables 2.6 and 2.7 also list SCFs as calculated using recent formulae[5,10,28] as well as the ratio of V-joint SCF to T-joint SCF, η. Although the small experimental values of α put the test specimens outside the proposed validity for the formulae, this fact should not be viewed as a major restriction on the use of the formulae here since the formulae either show little or no dependence on α. For example increasing α by a factor of two increase Kuang's chord SCF's by little more than 5%.

Gibstein's[10] and Wordsworth and Smedley's[28] chord SCF predictions were usually

Table 2.6 Stress Concentration Factors in Chord.

Specimen	Gibstein	Kuang	Wordsworth	Exp.	η_c
T1	22.25	23.50	23.50	16.06	
V1				33.07	2.06
T2	7.13	7.92	8.52	7.80	
V2				8.03	1.03
T3	17.96	16.21	18.42	14.41	
V3				8.29	0.57
T4	10.64	14.52	10.78	8.69	
V4				14.29	1.65
T5	12.48	13.53	14.02	16.38	
V5				16.66	1.01
V6				8.011	0.49
V7				11.87	0.72
T6	9.89	8.65	11.48	9.24	
V8				8.91	0.96
DT1				16.77	

within 30% of experimental values. Kuang et al's[5] predictions were generally slightly more accurate. Gibstein's formula for branch SCFs yielded results most consistent with experimental data. Kuang's and Wordsworth's predictions, on the other hand, were often in excess by more than 50%.

The highest strain recorded on V-joints always occurred at the chord exterior saddle, although specimen V6 had a simultaneous hotspot at the interior saddle. Low strains in the crotch region were recorded for all other specimens. High strain at 45° recorded on V2, a specimen with parametric values similar to one of Recho and Brozetti's[29] models, indicates the possible existence of a hotspot between 0° and 45°.

η_c varied from 0.5 to 2 while η_b varied from 0.3 to 1.6. This would indicate that the values of SCFs for V-joints can not be predicted with the T-joint formulae. Some

Table 2.7 Stress Concentration Factors in Branch.

Specimen	Gibstein	Kuang	Wordsworth	Exp.	η_b
T1	12.32	22.08	15.81	8.68	
V1				11.18	1.28
T2	6.27	10.04	6.36	7.20	
V2				4.62	0.64
T3	10.35	15.61	12.61	7.74	
V3				6.99	0.90
T4	7.63	15.90	7.79	4.75	
V4				7.70	1.62
T5	8.74	14.80	9.83	12.07	
V5				7.46	0.61
V6				4.62	0.38
V7				3.55	0.29
T6	7.92	8.99	8.23	4.79	
V8				7.42	1.54
DT1				5.49	

general trends seem to emerge from the chord SCFs. For instance, chord SCFs increase with increasing γ. The stress concentration factors however decrease with increasing β and up to a certain angle, with increasing ϕ. No such trends were observed with branch SCF mainly because of the low value recorded for specimen V7.

2.7.4 Chord Profile

The crown longitudinal profiles of T-joints offered little surprise. As expected, deflections were greatest at the branch-chord junction while only settlement was recorded at the support.

The crotch line profiles of the V-joints showed greater variations. Specimen V2 deflected downwards uniformly. Specimens V1, V4, V7, and V8 underwent greater deflections at the center of the specimen than at the loading points. This was expected

Figure 2.12 V-joint Profile after Collapse.

as the crotch is bulging outwards when collapse occurs (Fig. 2.12). A different type of profile was displayed by joints V3 and V5. The gap left between branches was too small to allow for bulging on the chord at the crotch. Consequently, greater deflections were recorded under the loading points than under the center of the joints. Profiles of V5 and V7 are shown in Fig. 2.13.

2.8 Experimental Conclusions

The following conclusions can be drawn from the results presented in this chapter:

(1) 90° V-joints are typically 3 to 4 times stiffer than corresponding T-joints. As ϕ increases or decreases the stiffness decreases as both branches tend to ovalize the chord in the same sense.

(2) T-joint strength formulae are generally conservative when applied to a V-joint. However, they seem to become overly conservative with high β values and uncon-

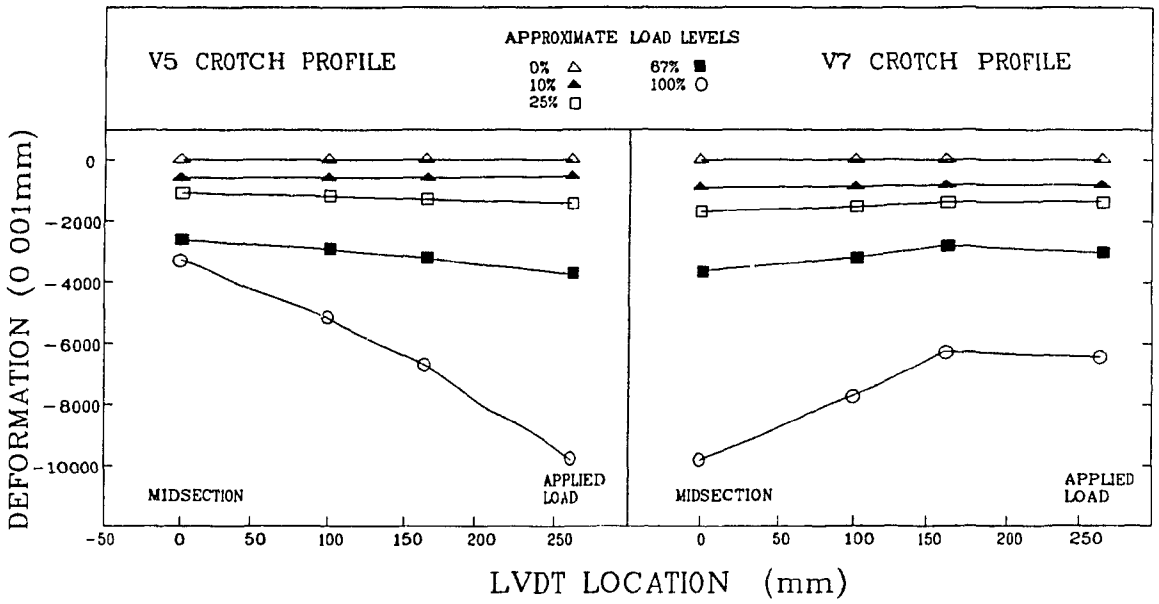

Figure 2.13 Experimental Crotch Line Profiles.

servative with ϕ greater than 90°.

(3) The AWS formula for multiplanar joints seems too generous in its predicted increase in strength for V-joints and does not adequately reflect loss of strength at angles greater than 90°.

(4) T-joint stress concentration factor formulae can not be used to predict V-joint-SCFs. although there is some similarity in the effects of geometric ratios.

(5) The hotspot always occurs on the back side of V-joints, most often at the saddle, while the stresses in the crotch region tend to be much lower.

CHAPTER 3

FINITE ELEMENT MODEL

3.1 Introduction

The Finite Element Method (FEM) is a powerful and popular numerical analysis technique. Its guiding concept is to divide the whole structure into a number of elements and to calculate the load vector and the stiffness matrix for each element. The element matrices and load vectors are then assembled into a global stiffness and a global load vector. A system of simultaneous equations can then be formed and solved for unknown nodal displacements. Stresses and strains are then obtained using interpolating shape functions and the constitutive stress-strain relations of the material.

A rigorous analysis of tubular joints requires the use of isoparametric shell elements but this was not the aim of this research. It was instead hoped to develop a predictive model based on the much simpler beam-column elements, thereby reducing computational costs, that would be able to reasonably predict the response of the loaded joint.

3.2 Basic Modelling Technique

This section will give a brief qualitative description of the model used in the program TUBE2D, which is a specialization of the nonlinear two-dimensional frame analysis program NAF2D[30].

The well known 2 node, 6 degree-of-freedom, (DOF), beam-column element is used in NAF2D. The element stiffness matrix is obtained by numerical integration since the closed form solution is abandoned due to the inclusion of material non-linearity. NAF2D uses the skyline technique to solve for unknown nodal parameters and provides two alternatives for reaching equilibrium at the end of each load increment. Those are the Newton Raphson Method (NRM) and the modified NRM.

A first attempt at modelling the joint was made using an unchanged NAF2D. The joint was represented by a ring of width d and thickness T as shown in Fig. 3.1. Only half of the ring need be considered because of symmetry. Since NAF2D uses straight beam elements the exact shape of the semi-circle cannot be reproduced. However, a close approximation can be obtained if a sufficient number of elements is used (36 elements were used in this study). The branch was not modelled but the load was applied at the two nodes which corresponded to the branch chord intersection at the mid-section of the joint. The lowermost node was fixed while the top node was allowed to translate downwards.

The joint behaviour as calculated from this simple model revealed three major discrepancies when compared to experimental evidence:

1) Very low collapse loads (when the solution fails to converge after a given number of iteration cycles).
2) Chord distortion between the points of load application.
3) First yield not at experimental hotspot.

Each of these shortcomings was studied and corrected.

The low ultimate resistance of the model is not surprising. It can be largely explained by the fact that the strength of the model was governed principally by the bending resistance of the ring rather than by the longitudinal bending resistance of the joint and the shearing resistance of the chord cross-section as observed in the actual case. To provide the missing resistance components, each element could be supported

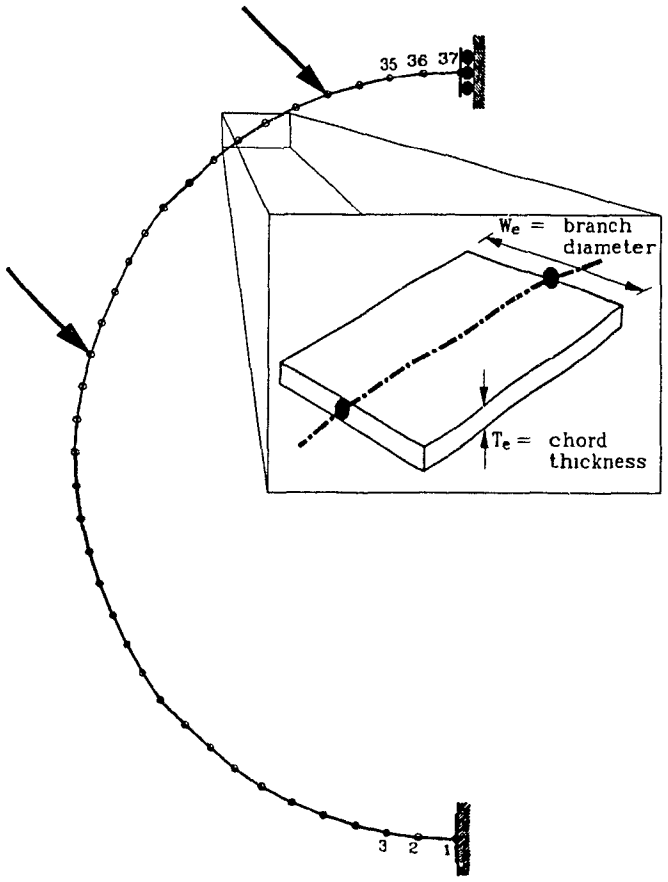

Figure 3.1 NAF2D Ring.

on elastic foundations i.e. each element can be formulated as a beam-column resting on continuous normal and tangential springs.

The great chord distortion between the points of load application that was observed in the NAF2D run does not occur in reality since it is prevented by the high stiffness of the branch. In order to simulate the branch stiffening effect, it was decided to use a thickness of 10T between the point loads in the model.

Finally the fixity of the bottom node precipitated yielding in the lower elements which was contrary to the experimental evidence which indicated that yielding first occurred near the branch. The insertion of the elemental springs provided a distributed resistance in the downwards direction so that the bottom node could also be placed on

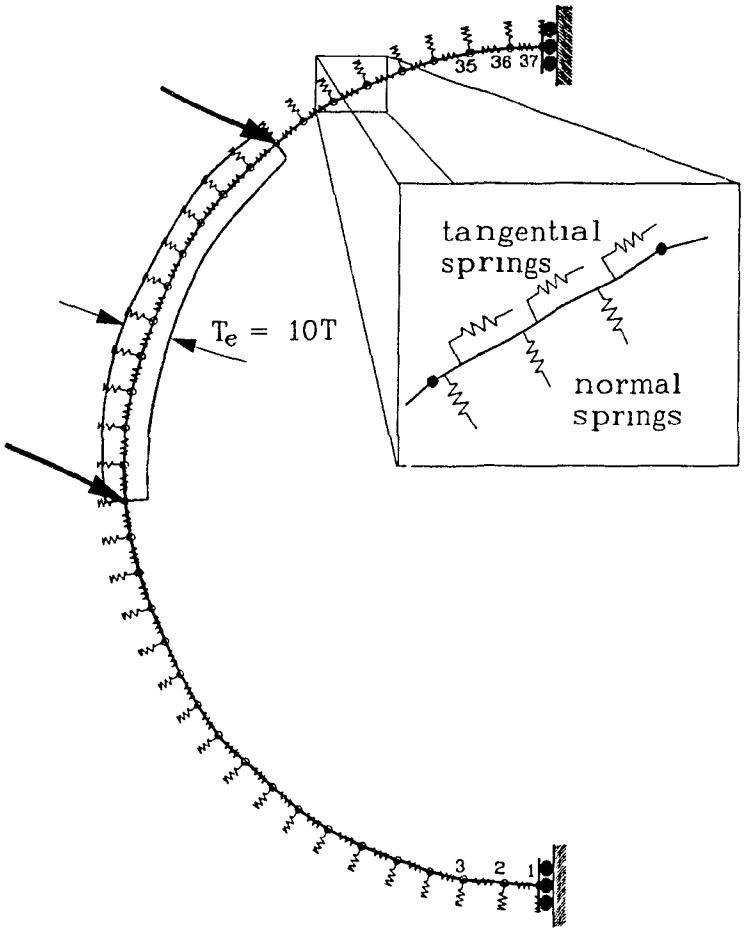

Figure 3.2 TUBE2D Model.

rollers thus preventing stress build-up at that node. The changes made as a result of the NAF2D runs provided the basic qualitative model shown in Fig. 3.2 which is used in program TUBE2D.

3.3 Element Formulation

The detailed formulation of the well-known beam-column element used in NAF2D and shown in Fig. 3.3 can be found in previous work by Mitri[30]. The dimensions of the element are specified as:

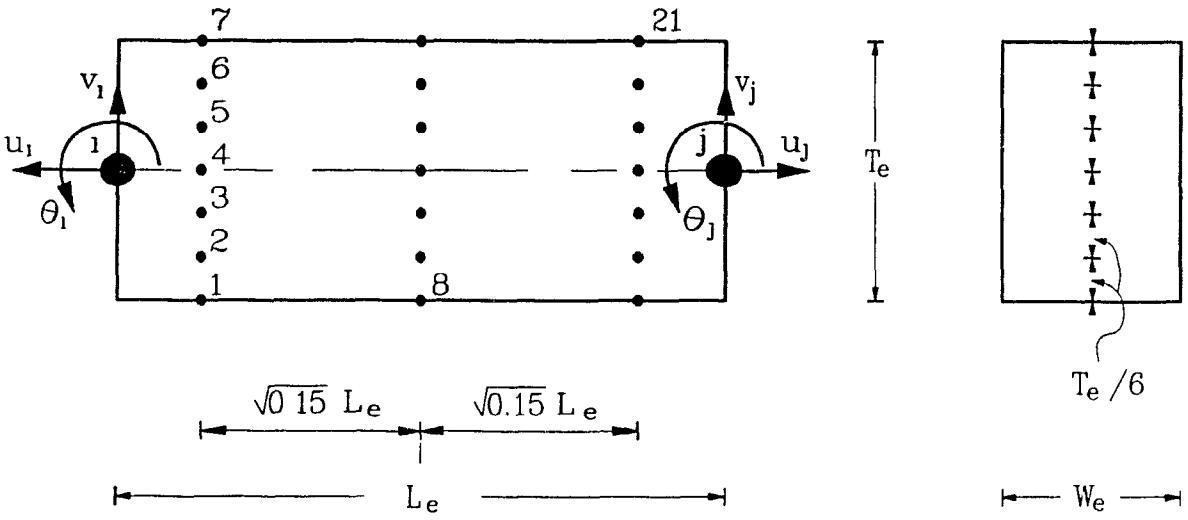

Figure 3.3 NAF2D Beam-Column Element[30].

(a) L_e element length,

(b) T_e element thickness, and

(c) W_e element width.

The element has six degrees of freedom and its stiffness matrix is numerically intergrated over 21 sampling points. This section will focus on the tangential and normal spring stiffnesses which were added to the beam-column element in TUBE2D. The total element stiffness matrix $[K^t]$ is obtained from the algebraic addition of its two components, i.e.:

$$\underset{6\times6}{[K^t]} = \underset{6\times6}{[K_{NAF}]} + \underset{6\times6}{[K_{sp}]}$$

where $[K_{NAF}]$ is the element stiffness matrix from NAF2D, and

$[K_{sp}]$ is the element spring stiffness matrix.

The spring stiffness is made up of two basic components; K_t, the tangential spring stiffness per unit length and K_n, the normal spring stiffness per unit length. The

element spring stiffness is derived from strain energy considerations. It can then be calculated by integrating over the element length as follows:

$$\underset{6\times6}{[K_{sp}]} = \int_{L_e} \underset{6\times2}{[N]^T} \begin{bmatrix} K_t & 0 \\ 0 & K_n \end{bmatrix} \underset{2\times6}{[N]}\, dx$$

where [N] is the shape function matrix.

$$[N] = \begin{bmatrix} N_1^c & 0 & 0 & N_2^c & 0 & 0 \\ 0 & N_1^b & N_2^b & 0 & N_3^b & N_4^b \end{bmatrix}$$

where the superscript c refers to column displacement and superscript b to beam actions. The shape functions are defined as:

$$N_1^c = \frac{L_e - x}{L_e}$$
$$N_2^c = \frac{x}{L_e}$$
$$N_1^b = 1 - \frac{3x^2}{L_e^2} + \frac{2x^3}{L_e^3}$$
$$N_2^b = x - \frac{2x^2}{L_e} + \frac{x^3}{L_e^2}$$
$$N_3^b = \frac{3x^2}{L_e^2} - \frac{2x^3}{L_e^3}$$
$$N_4^b = \frac{-x^2}{L_e} + \frac{x^3}{L_e^2}$$

The closed form of the spring stiffness is obtained after integration

$$[K_{sp}] = \begin{bmatrix} \frac{L_e}{3}K_t & 0 & 0 & \frac{L_e}{6}K_t & 0 & 0 \\ 0 & \frac{13L_e}{35}K_n & \frac{11L_e^2}{220}K_n & 0 & \frac{9L_e}{70}K_n & \frac{-13L_e^2}{420}K_n \\ 0 & \frac{11L_e^2}{220}K_n & \frac{L_e^3}{105}K_n & 0 & \frac{13L_e^2}{420}K_n & \frac{-L_e^3}{140}K_n \\ \frac{L_e}{6}K_t & 0 & 0 & \frac{L_e}{3}K_t & 0 & 0 \\ 0 & \frac{9L_e}{70}K_n & \frac{13L_e^2}{420}K_n & 0 & \frac{13L_e}{35}K_n & \frac{-11L_e^2}{220}K_n \\ 0 & \frac{-13L_e^2}{420}K_n & \frac{-L_e^3}{140}K_n & 0 & \frac{-11L_e^2}{220}K_n & \frac{L_e^3}{105}K_n \end{bmatrix}$$

The values of K_t and K_n must be determined in order to completely define $[K_{sp}]$ and properly calibrate the model. The spring constants per unit length of the element in TUBE2D are set equal to the bending and shear stiffness of an elastic strip spanning the joint length L and subject to a concentrated load at midspan, i.e.:

$$K_n = 48\frac{EI}{L^3}$$
$$K_t = 4\frac{AG}{L}$$

where:

E, G	are Young's and shear modulii of elasticity,
L	is the full length of the joint,
A, I	are the area and moment of inertia of the strip considered as shown in Fig. 3.4. Note that $A = 1 \times T_e$ and $I = 1 \times \frac{T_e^3}{12}$.

3.4 Equations of Equilibrium

In the linear range $[K_{NAF}]$ is obtained and added to $[K_{sp}]$ to yield the element equation of equilibrium:

$$\underset{6\times6}{[[K_{NAF}] + [K_{sp}]]} \; \underset{1\times6}{\{\Delta\}} = \underset{1\times6}{\{P\}}$$

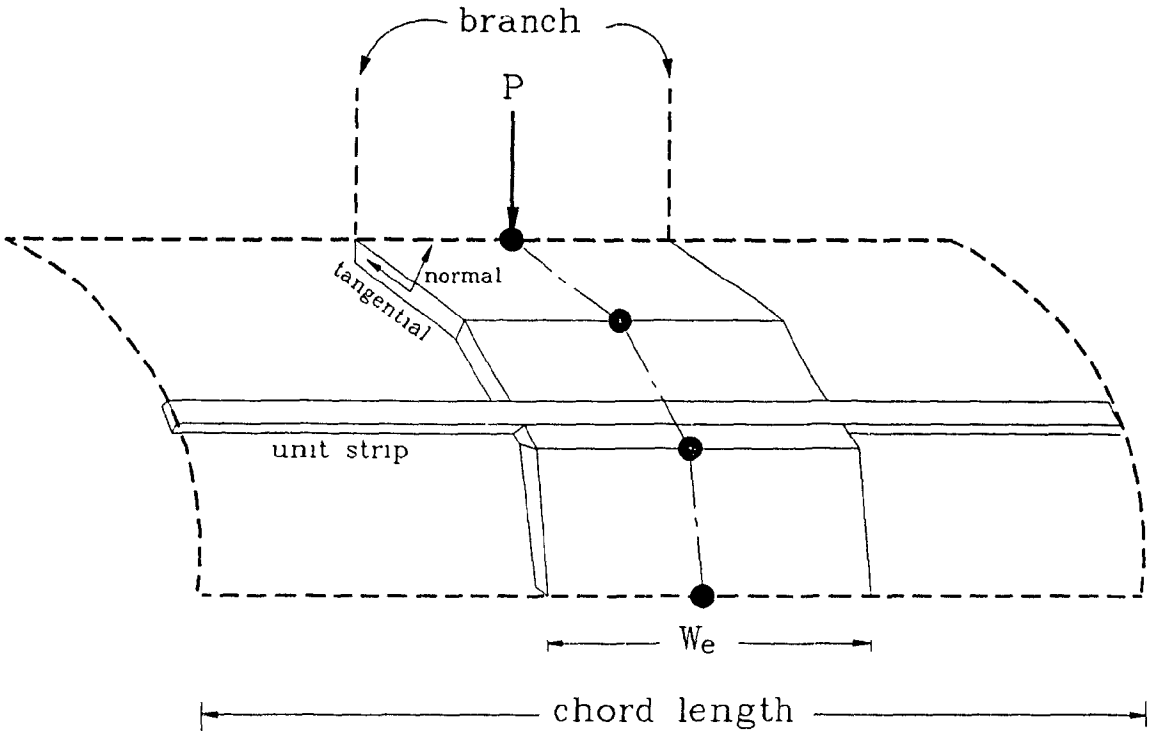

Tangential dir $\quad K_t = \frac{48EI}{L^3} \equiv \frac{48E}{L^3}\frac{T_e^3}{12}$

Normal dir $\quad K_n = \frac{4AG}{L} = 4\,T_e\,\frac{G}{L}$

Figure 3.4 Spring Constant Definitions.

where: $\{\Delta\}$ contains the nodal displacements,

$\{P\}$ is the load vector.

In the non-linear range the stiffness matrix is determined at each load step. Since the Newton Raphson Method was used, the stiffness matrix was updated at each iteration before solving for stresses, strains, and displacements. The discretized equations of equilibrium after m iterations in the n^{th} load increment can be expressed as:

$$\{\psi_n^m\} = \{R_n^m\} - \left\{\sum[\int_v [B]^T \sigma_n^m dv + [K_{sp}]\{\Delta\}]\right\}$$

where [B] is the beam element strain matrix so that $\sum[\int_v [B]^T \sigma_n^m dv + [K_{sp}]\{\Delta\}]$ is the

total resistance offered by the joint model. The quantity

$\{R_n^m\}$ is the consistent load vector due to externally applied loads,

while $\{\psi_n^m\}$ is the unbalanced load vector.

Iterations are stopped when the increment in internal energy during the m^{th} iteration ΔW_n^m divided by the initial work done by the out of balance forces ΔW_n^o is less than a specified tolerance. In TUBE2D, the iteration is limited when

$$\frac{\Delta W_n^m}{\Delta W_n^o} < 0.001$$

3.5 Material Model

Program TUBE2D includes non-linear material behaviour for the beam-column element but the springs are assumed to remain elastic. Geometric nonlinearities are not included so that deformation predictions are limited to small deflections. It is to be noted that V-joints reached their ultimate strength at deflections less than half their chord thicknesses whereas most T-joints underwent deformations of approximately the same magnitude as their chord thicknesses, a range at which small deformations theory may be no longer be safely relied upon.

The steel properties used are those which were experimentally determined. The stress-strain curve is idealized as bilinear with slopes E and E_T to account for strain hardening. If the normal stress reaches the ultimate stress σ_{ult}, no further strain hardening is allowed and hence $E_{ij} = 0$. The bilinear relationship used is shown in Fig. 3.5.

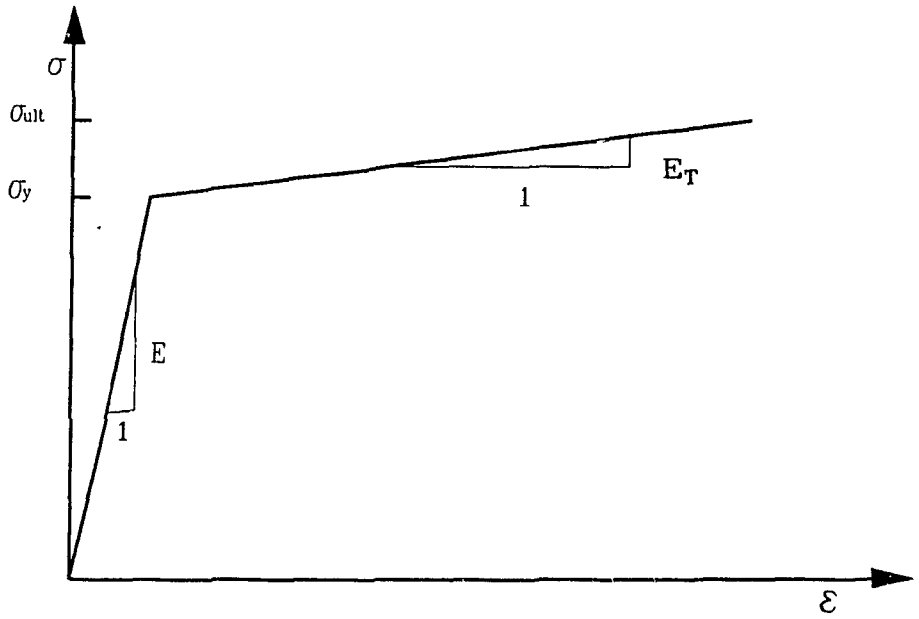

Figure 3.5 Idealized Material Model.

CHAPTER 4

MODEL VERIFICATION

4.1 Introduction

An ideal FEM model should be able to completely predict the response of the structure it represents. This would include complete load-deformation curves and stress and strain values at any point in the structure. A simple 2D model such as TUBE2D can not pretend to such precision but it would be useful if it could predict the early part of the load-deformation curve and the location of the hotspot.

4.2 Model Stability

Before comparing numerical predictions to experimental values, the effect of the number of elements, the analysis method and the tangent modulus value must be ascertained.

As mentioned in Chapter 3, 36 elements were deemed sufficient to give a close approximation to a circular shape. Comparison with a tube of 72 elements is shown in Fig. 4.1. The 72 element model yields sooner and is generally 10% weaker than the 36 element one. Computation time however is more than doubled.

TUBE2D can use either the Newton Raphson Method or Modified Newton Raphson Method as a solution technique in the non-linear range. Fig. 4.2 shows that results

are independent of which procedure is selected. A series of computer runs was then made with varying tangent modulii. Results with $E_T = 0$, 2000, 4000 and 8000 MPa can be seen in Fig 4.3.

As can be expected the higher tangent modulii produced higher resistance joints although there was more stiffening of the response between $E_T = 0$ and 2000 MPa than between $E_T = 2000$ and 8000 MPa. It should be noted that all computer simulations show a consistent increase of strength with increased deformation; this is simply due to the fact that the springs in the TUBE2D model remain elastic. A value of $E_T = 2000$ MPa was selected for all runs as it approximated experimental values obtained in the coupon tests and gave closest agreement when modelling the control joint, i.e., specimen V7.

4.3 Comparison with V-joint Experimental Results

The analytical model having been completely defined its results can then be compared to experimental data. Excellent agreement is achieved with V7 where the predicted deflections are within 10% of the measured deflections until the applied load P exceeds 90% of the ultimate load P_u. This can likewise be interpreted as the predicted P being within 10% of the experimental P until the branch penetration reached 1 mm. This limit of 1 mm or approximately 1% of R, appears to be the deformation value at which the spring stiffness begins to unduly govern the response of the model.

The response of the other two joints in the γ series, V1 and V2, was also predicted well by TUBE2D with deformation values again staying within 10% of experimental values at loads less than 90% P_u. The prediction of V2 is especially good: at 1 mm deformation the predicted load is within 2% of the experimental one. The theoretical and experimental load-deformation curves of the γ series are shown in Fig 4.4. Figure 4.5 compares the load deformation TUBE2D predictions to the experimental curves obtained when studying the β series. The curves are qualitatively correct; V4 shows

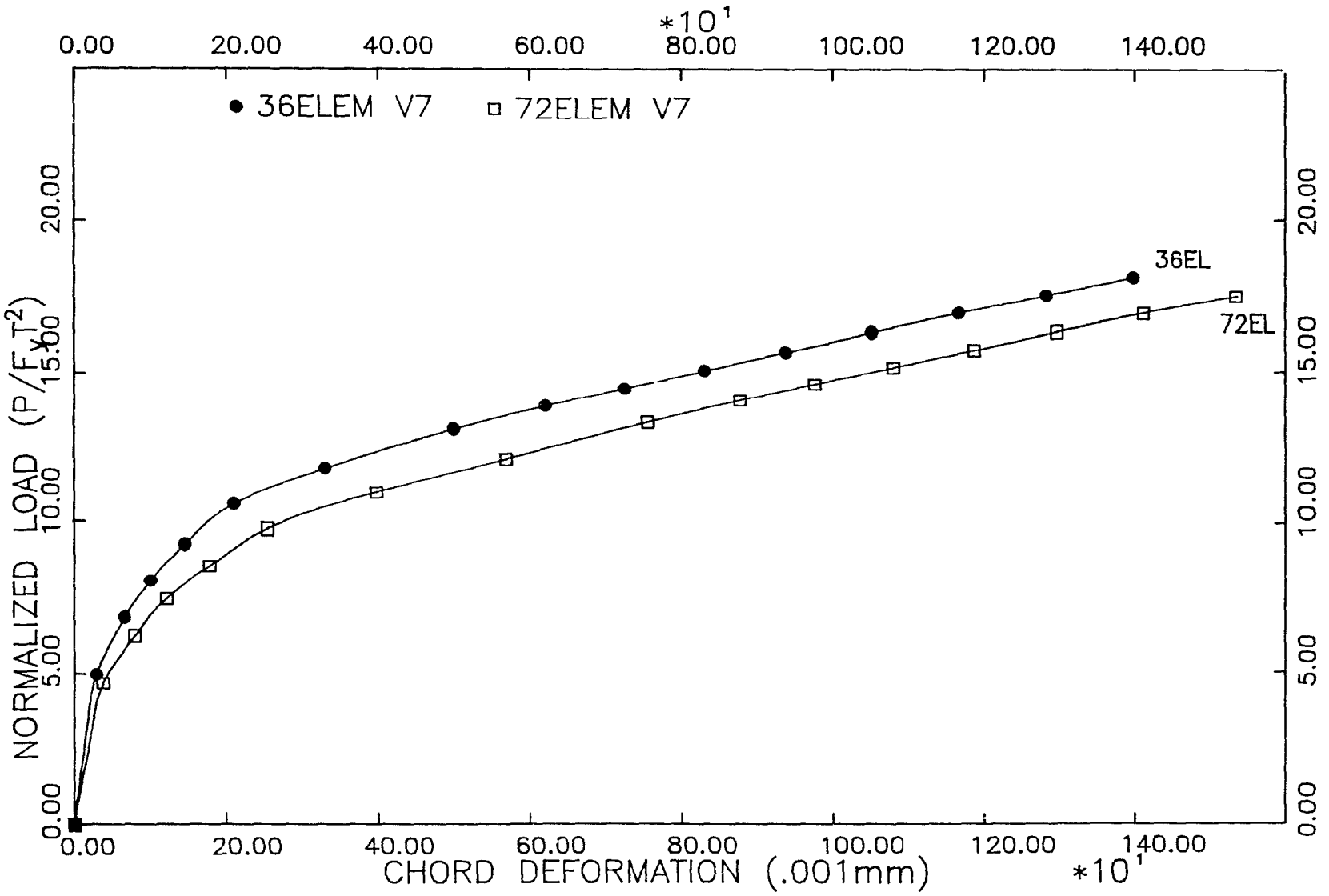

Figure 4.1 Effect of Number of Elements on Predicted Load-Deformations Curve.

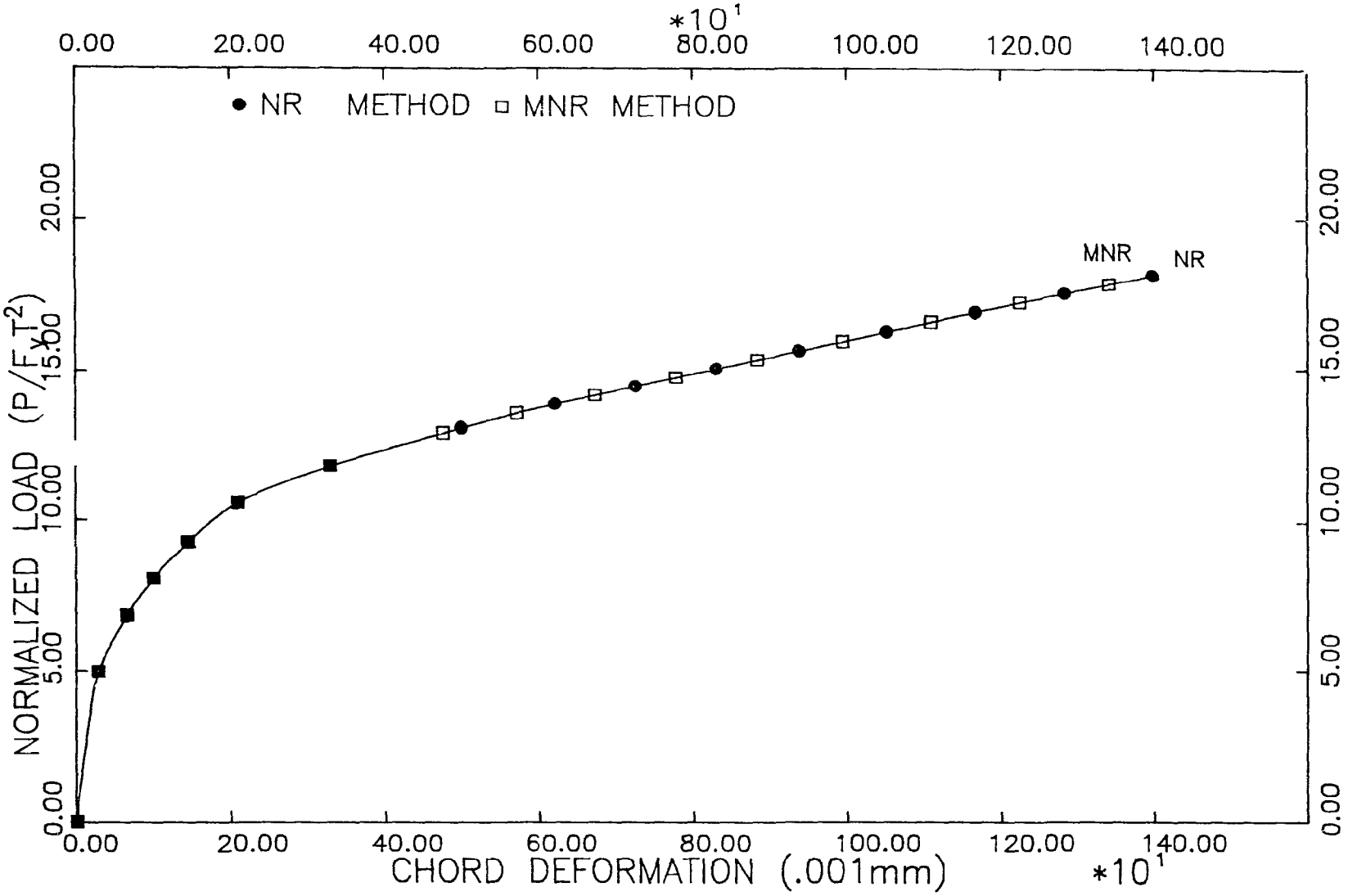

Figure 4.2 Effect of Analysis Method on Predicted Load-Deformation Curve.

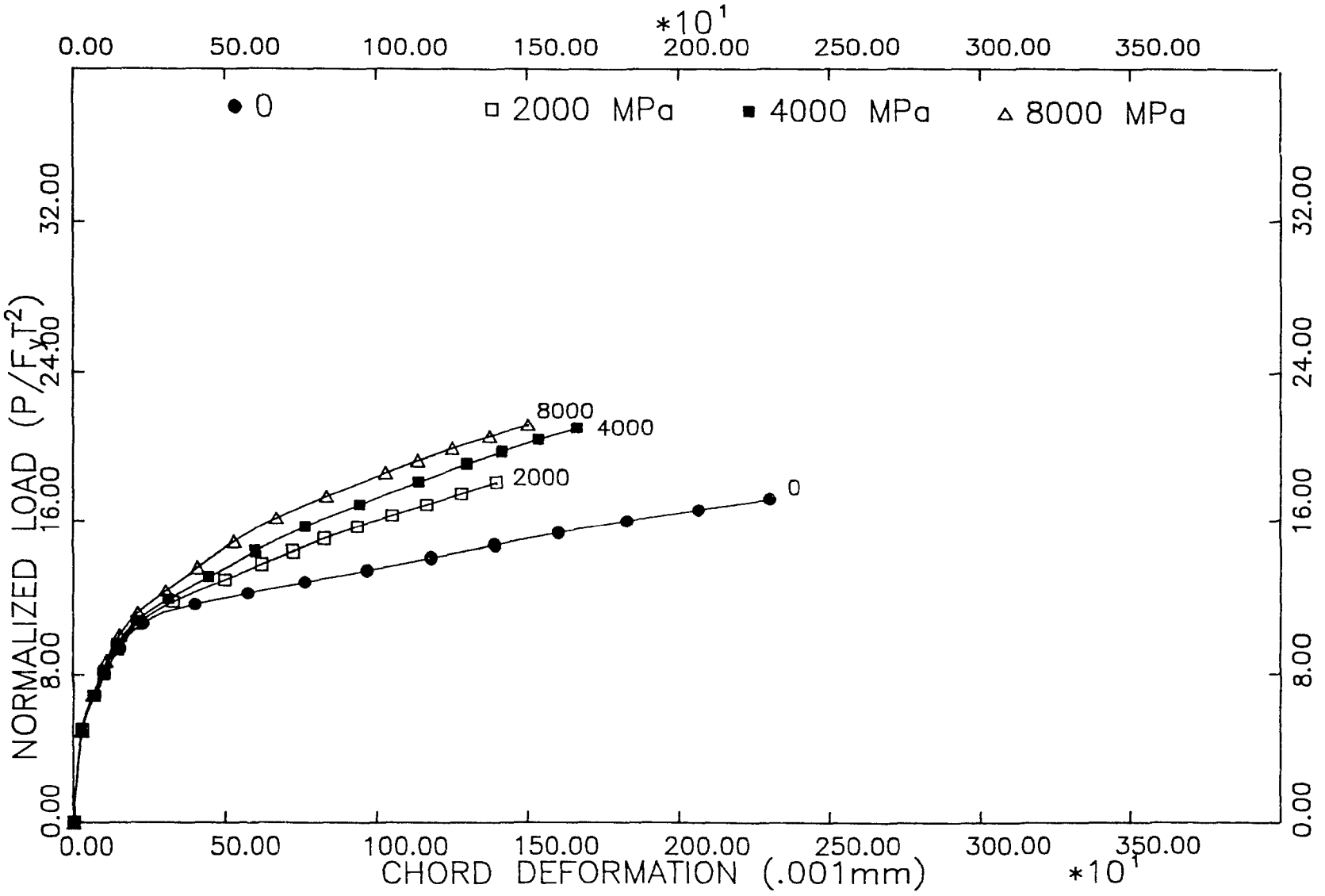

Figure 4.3 Effect on Tangent Modulus on Predicted Load-Deformation Curve.

the weakest response, V7, is in the middle while V3 towers above both of them. The computed response of V3 shows some negative penetration (axial elongation) as was recorded during the experiments.

Although qualitatively correct the β response curves shown in Fig. 4.5 are not as accurate as those of the γ series shown in Fig. 4.4. Indeed the V4 model underpredicts the load in the joint for any given deformation e.g. at 1 mm branch penetration the model predicts only 75% of the resistance that was measured during testing. It is to be noted that the experimental response of V4 was the only one that was underpredicted by the model

The uniqueness of the response of joint V3, makes comparison with the response predicted by TUBE2D more difficult. The model did predict axial elongation although only 20% of that measured in the experiment. TUBE2D predicted a transition from elongation to penetration at a load level equivalent to 85% of the experimental ultimate load.

Figure 4 6 presents the model predictions for V-joints in the ϕ series. The least success was achieved in predicting the response of the non 90° V-joints. The computer model predicted a stronger and stiffer response from V6 than from V7 which is contrary to experimental evidence Higher resistance is predicted for both V6 and V5 where the predicted resistance at 1 mm deformation is more than twice the observed resistance and higher than the actual ultimate strength Although stiffer than the experimental specimen the V5 model did exhibit the most flexible initial response of the V-joints just like its comparable experimental joint.

Every computer run properly located the hotspot at the outside intersection of branch and chord. Calculations of SCFs are slightly misleading since the branches are only represented by loads and not actual elements. Nevertheless by dividing the computed branch load by experimental branch area the SCFs listed in Table 4.1 were obtained. It can easily been seen that qualitative agreement is best with the γ series

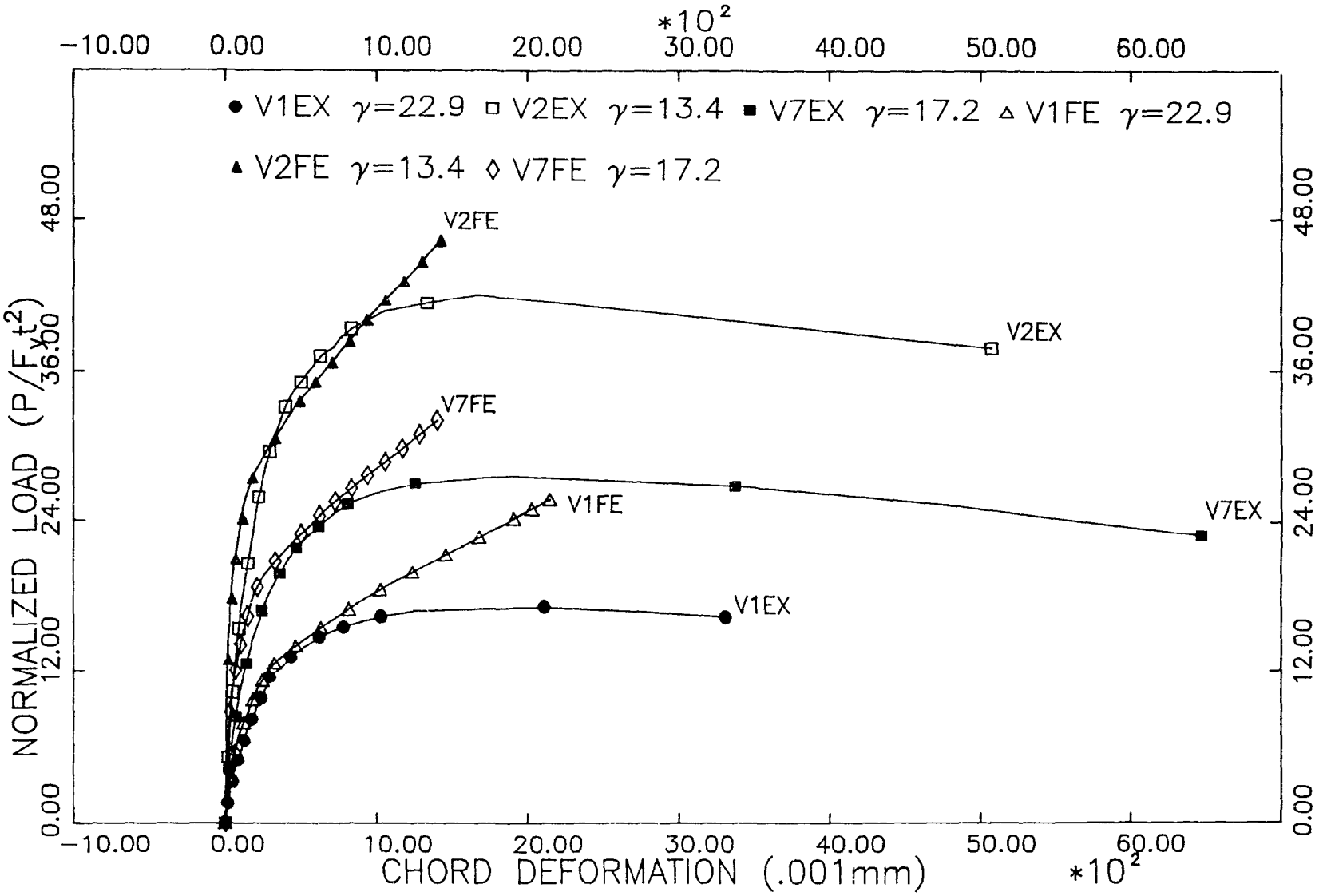

Figure 4.4 Comparison of Experimental and Predicted Load-Deformation Curves for γ Series V-joints

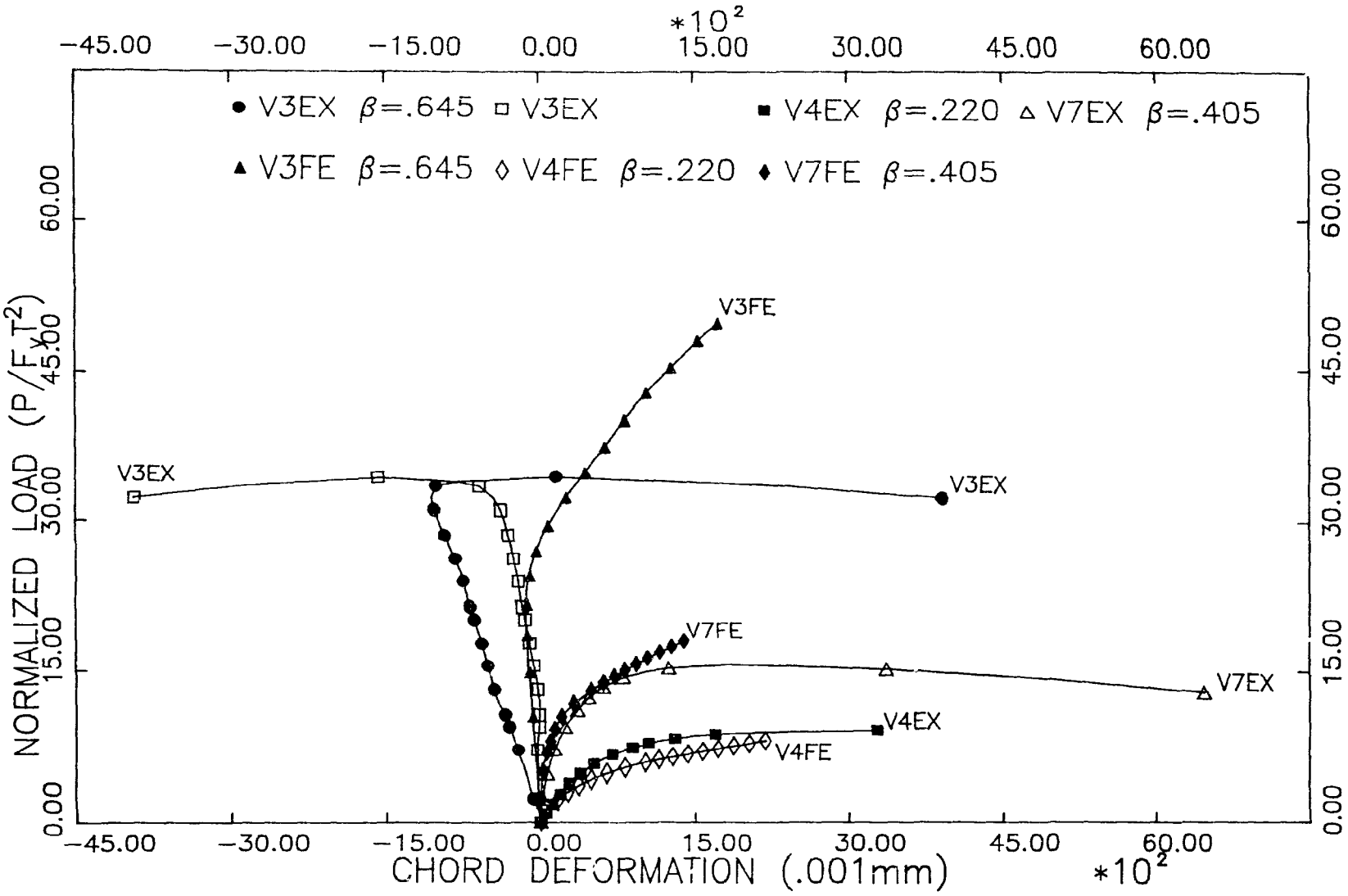

Figure 4.5 Comparison of Experimental and Predicted Load-Deformation Curves for β Series V-joints.

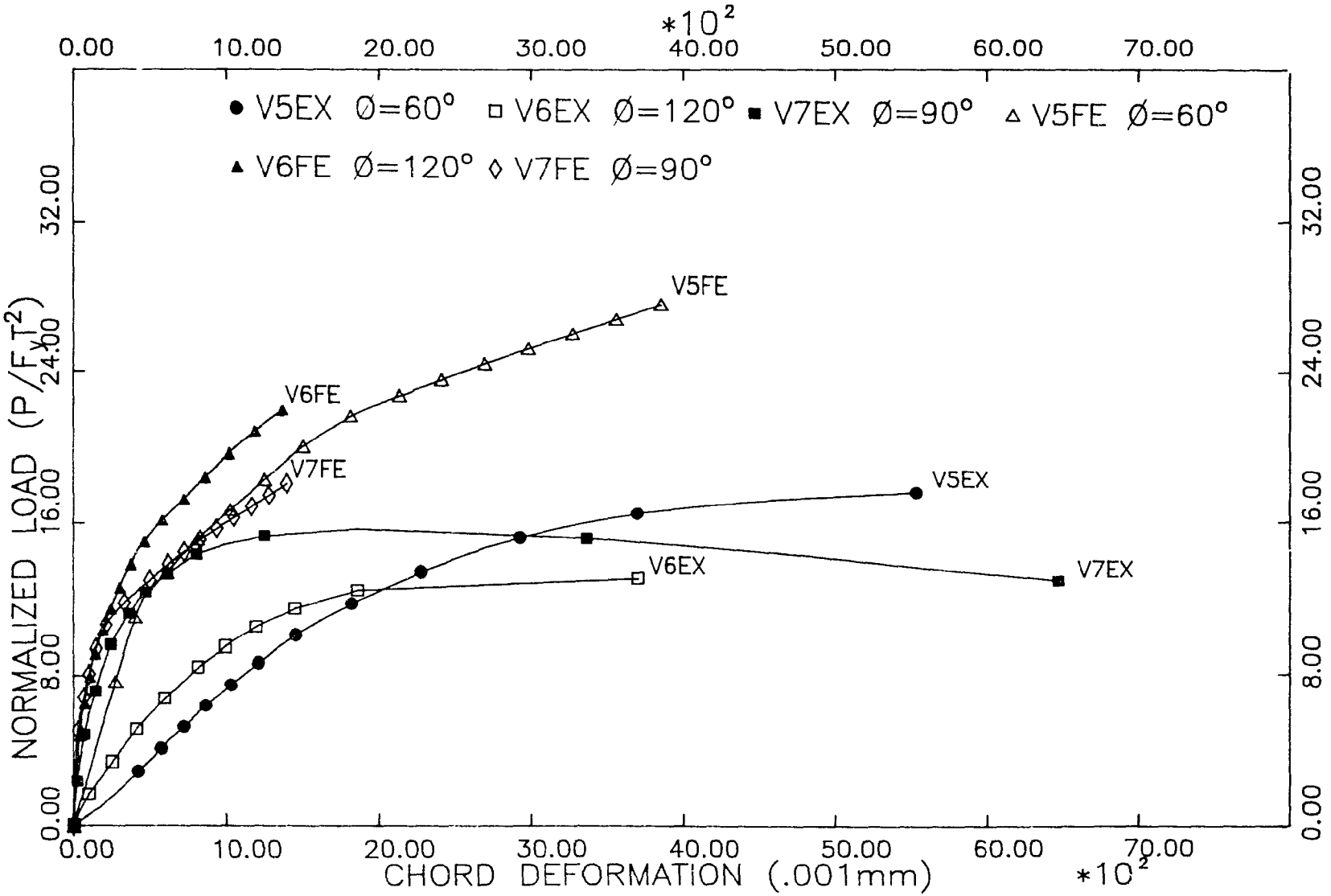

Figure 4.6 Comparison of Experimental and Predicted Load-Deformation Curves for ϕ Series V-joints.

which shows a sharp reduction in SCFs with increased chord thickness. The β series does exhibit an increase in SCFs with reduction of β but the trend is a lot weaker than the one observed experimentally. Finally the computer results for the ϕ series are again contradicted by experimental observations.

Table 4.1 Stress Concentration Factors in V-joint Chord.

Specimen	Model	Experimental
V1	15.83	33.07
V2	6.90	8.03
V3	10.60	8.29
V4	12.45	14.29
V5	5.75	16.66
V6	10.85	8.01
V7	10.26	11.87

4.4 Comparison with T-joint Experimental Results

The T-joints which were tested for comparative purposes were also modelled using TUBE2D. The load-deformation curves predicted by the model are presented in Fig. 4.7 for the β series and Fig. 4.8 for the γ series along with the comparable experimental results.

Both figures lead to the same conclusions and comments. For both the β and the γ series the model follows the experimentally observed trend. The joint in the β series showed an increase in strength with increasing β whereas the joints in the γ series showed a decrease in strength and stiffness with increasing γ. However, the predicted load-deformation curve for all T-joints exceeded experimental curves by a factor varying between 2 and 5. In fact the TUBE2D computed T-joint responses which were generally only 10% below those it computed for V-joints.

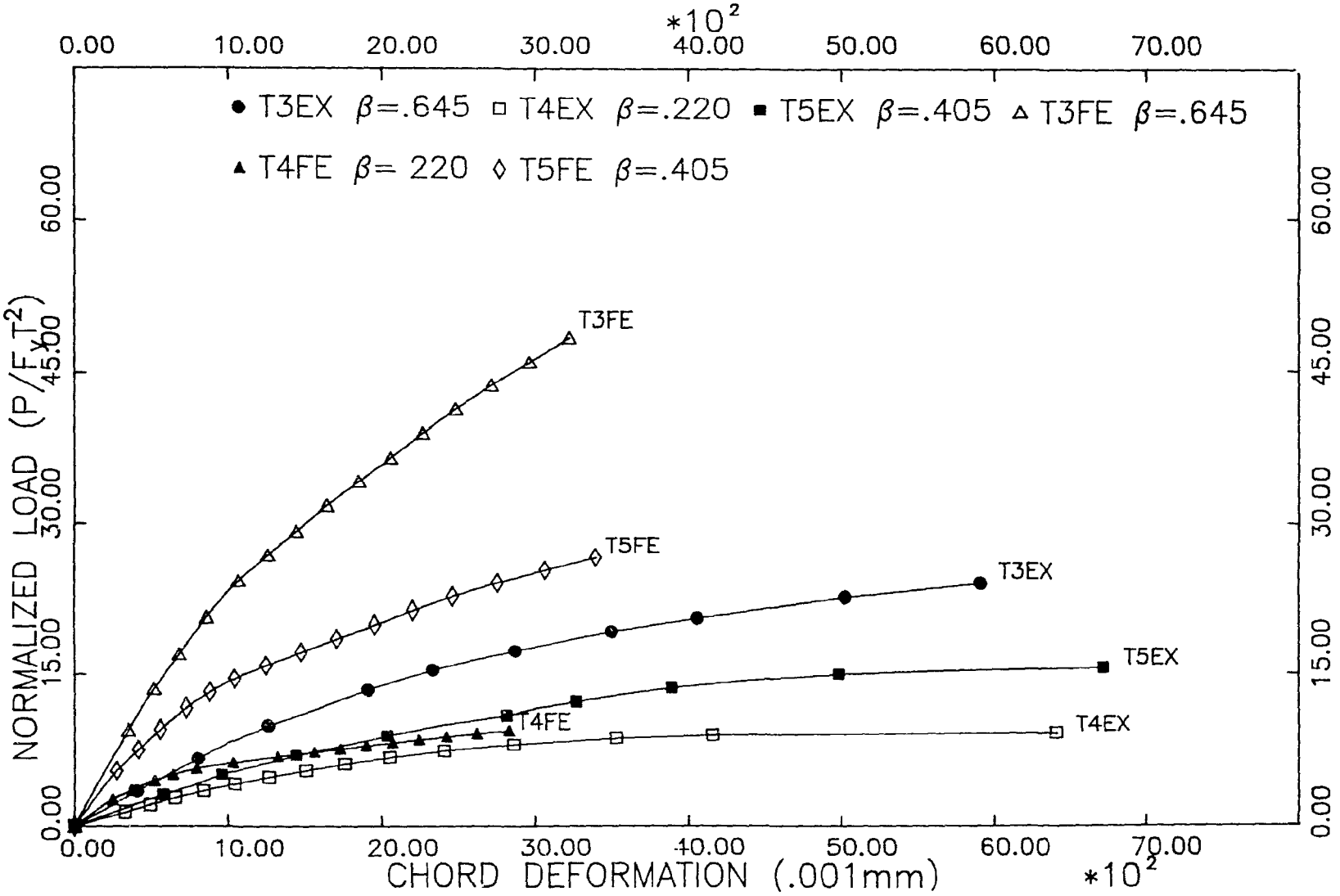

Figure 4.7 Comparison of Experimental and Predicted Load-Deformation Curves for β Series T-joints

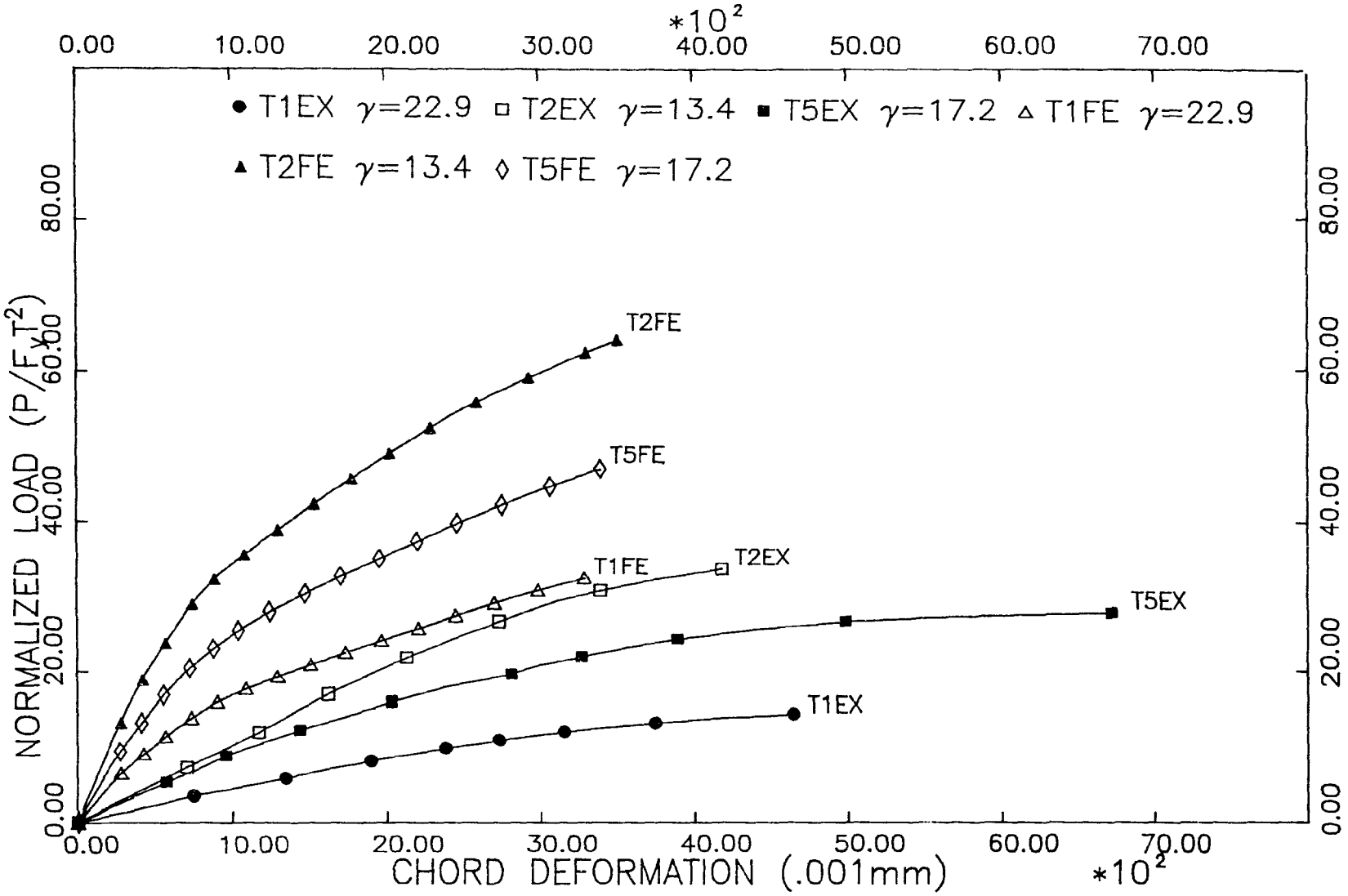

Figure 4.8 Comparison of Experimental and Predicted Load-Deformation Curves for γ Series T-joints.

The predicted SCFs factors also were very similar to those obtained in the V-joint analyses as can be seen in Table 4.2. Once again it is the γ series which yields the best results with both T1 and T2 predicted SCFs being within 15% of experimental values. Values of SCF calculated by TUBE2D were generally 20 to 40 percent lower than similar values calculated in Chapter 3 using the formulae of Gibstein[10], Kuang et al[5] and Wordsworth and Smedley[28].

Table 4.2 Stress Concentration Factors in T-joint Chord.

Spe imen	Model	Experimental
T1	14.04	16.06
T2	6.66	7.80
T3	11.64	14.41
T4	11.07	8.69
T5	9.49	16.38

4.5 Proposed Changes to TUBE2D

TUBE2D produced excellent predictions for 90° V-joints. However the poor agreement obtained between the experimental and TUBE2D predictions for V5, V6 and the T-joints require some model modifications to be made before it can be relied upon for use in the analysis of axially loaded tubular joints.

The poor agreement mentioned above mostly affected joints which were evidently more flexible than 90° joints and consequently more likely to suffer loss of stiffness due to geometric nonlinearities. The inclusion of these effects in TUBE2D would soften the model response and yield better correlation between experimental and theoretical results.

Another change to the model would be the addition of non-linearity to the spring stiffnesses. Yielding in the spring would permit the model to reach a peak value of load and therefore might allow for a longer part of the load-deformation curve to be closely reproduced.

CHAPTER 5

TUBE ANALYSIS SYSTEM

5.1 Introduction

The TUBE ANALYSIS SYSTEM software package, TAS, was developed to facilitate the use of the finite element program TUBE2D. All of the sub-units in TAS have been written in ASCII Fortran 77 and compiled with Microsoft Fortran 3.31. The graphical processors call on subroutines from the McGill Plotting Package Subroutines (MPPS)[35] and Jeffrey's[36] FORTPLOT Library, and are device independent provided that the appropriate device drivers are installed. The TAS system was designed mainly to operate on IBM compatible personal computers equipped with a fixed disk and a mathematical coprocessor.

TAS is composed of six basic modules which are indicated as rectangles in the system's flowchart shown in Fig. 5.1. The first two modules, TUBGEN and DATACK are preprocessors which interactively create a datafile and display the geometry on screen. The third module, program TUBE2D, is the core processor of the system. The next two units, PENLOAD and SHAPE are displacement post-processors. The VIEW utility from the FORTPLOT Library completes the system by allowing reproduction of files produced by the graphical processors.

TUBGEN is a data generating program for the core program TUBE2D. TUBGEN

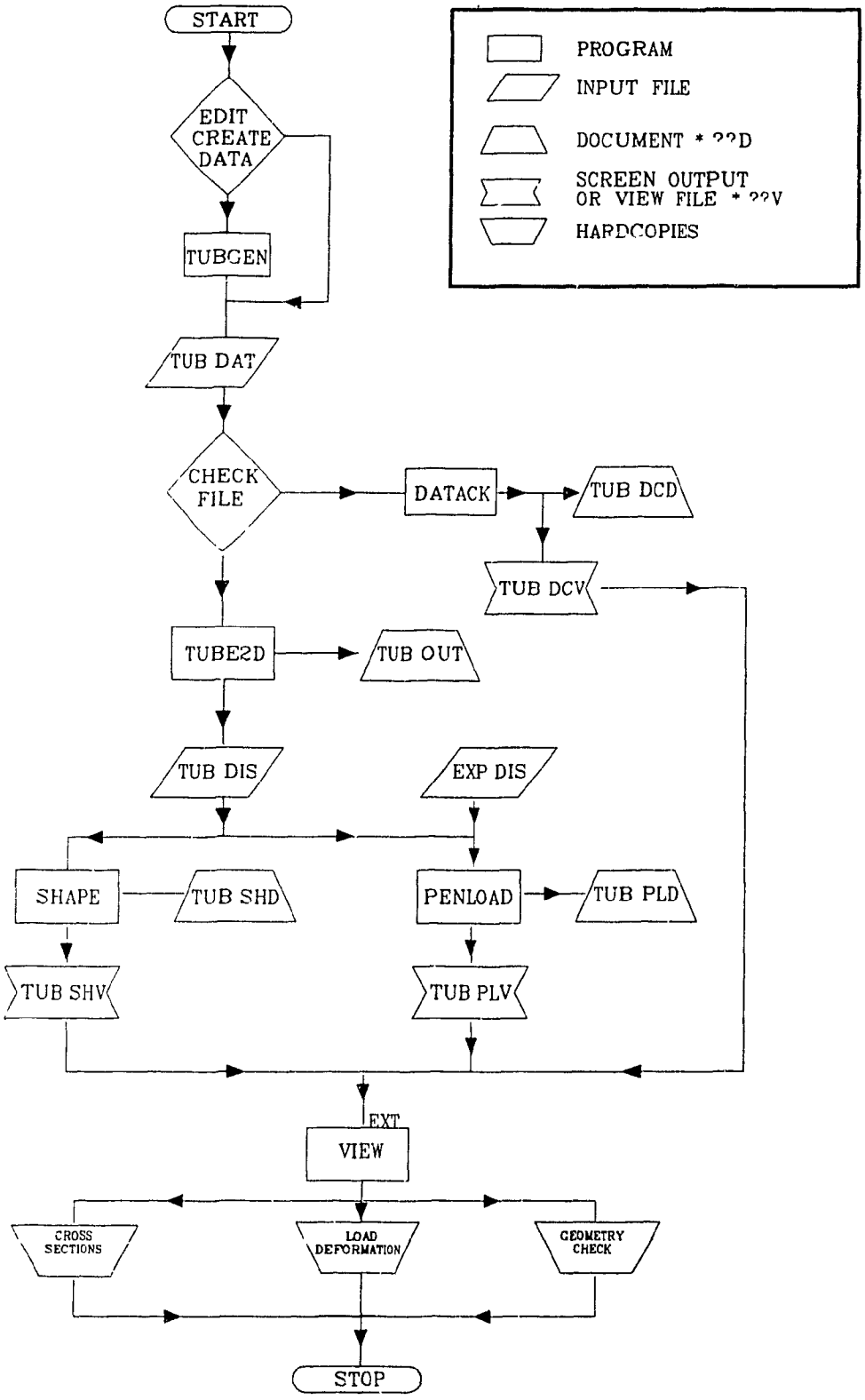

Figure 5.1 TUBE ANALYSIS SYSTEM (TAS) Flowchart.

prompts the user for all the information needed to generate a full input file. Among the specific data the user is asked to supply are the number of nodes, the radius of the tube, the element and the material properties, and the loading conditions. TUBGEN can also be used to edit an existing data file.

DATACK is a preprocessor which allows for a graphical check of the input data. It is particularly recommended to check input files which were not created with TUBGEN. In addition, DATACK outputs a document file which gives all input data for TUBE2D as well as showing both polar and rectangular coordinates of each nodal point. It should be noted that only one set of coordinates is required in the input file.

TUBE2D is the finite element core of the TAS system. Joints are modelled by a series of beam elements continuously supported by continuous springs as described in Chapter 3. TUBE2D generates two output files. The first output file can include, at the user's discretion, all loads and displacements as well as the stress values at each integration point in the yielded elements. The second document file contains only displacements and loads output and is formatted to be used as an input file for the post-processors.

PENLOAD is a graphical post-processor which reads the displacement output file and generates load-deformation curve. PENLOAD can read up to seven different input files and plot the resulting curves on the same graph for comparison purposes.

SHAPE is a second graphical post-processor. It uses the displacement output file to generate the deformed shape of the cross-section at various load levels. The cross-sections can be displayed one, two, or four at a time and the displacements can be shown with any selected magnification.

Both post-processors can generate their output on the screen or store it in a VIEW file. The VIEW utility can then be used to display the file as many times as required on a terminal screen or to create a hardcopy on a plotter or printer.

5.2 Solution Procedure

A flowchart of the basic structure of TAS is shown in Fig. 5.1. The solution procedure is described as follows:

1. Prepare a data file, TUB.DAT, for the core program TUBE2D. This data file can either be created by manual input of all data with a text editor or generated interactively by using TUBGEN.
2. The user has the option to verify his input data through the visual check available with DATACK.
3. Run TUBE2D to produce the two output files TUB.OUT and TUB.DIS. The former is the documentary output file while the latter is to be the input file for the graphical postprocessors.
4. Produce the load-deformation curves and deformed shape with PENLOAD and SHAPE. The graphical output can be viewed on screen or stored in a VIEW file for further reproduction.
5. View the graphical output on the screen, or create a hardcopy on a plotter or printer.

5.3 Using TAS

The interactive nature of TAS makes the software package easy to learn and to use. All filename extensions are standardized as shown in Fig. 5.1 and are automatically generated. Although the prompts which appear on screen are generally straightforward, certain module characteristics need to be described more fully.

5.3.1 TUBGEN

The tube model is generated clockwise with the zero degree node having coordinates (0,-R). A data file created by TUBGEN must be edited before it serves as input for TUBE2D. The edit function in TUBGEN which divides the data file into five

blocks- general, nodal, elemental, load, and end – can be used for that purpose. In particular, the following three points need to be looked at when editing:

1) Program mode,

2) Degrees of freedom,

3) Element thickness.

The program mode is originally set at 0 for data-check only, it should eventually be changed to 3 for elastic-plastic solution. When the data file is created all nodal degrees of freedom are set free The user must ensure the proper boundary conditions are described. When TUBGEN first generates the tube it sets all element thickness to the given chord thickness As indicated in Chapter 3 a thickness of 10T for chord elements under the branch provides for the stiffness of the branch

As previously mentioned the edit function in TUBGEN can be used to effect these changes. The TUBGEN editor allows for both horizontal (i.e changing all data for one given element or node) or vertical (i.e. changing one data for a group of elements or nodes) data entry. Whenever horizontal changes are underway TUBGEN prompts with the existing data

5.3.2 DATACK

DATACK is one of the easiest module to run in TAS. It only inquires about input and output files and devices. DATACK generates one screen The screen displays the problem title as well as all nodes in location, numbered and showing their degree of freedom. Also displayed are the actual loads in their proper orientations as shown in Fig. 5.2. DATACK will warn the user if the program mode is not equal to three, if all degrees of freedom are free or if all element thicknesses are the same.

5.3.3 TUBE2D

The core processor is also limited to prompts concerning input and output files.

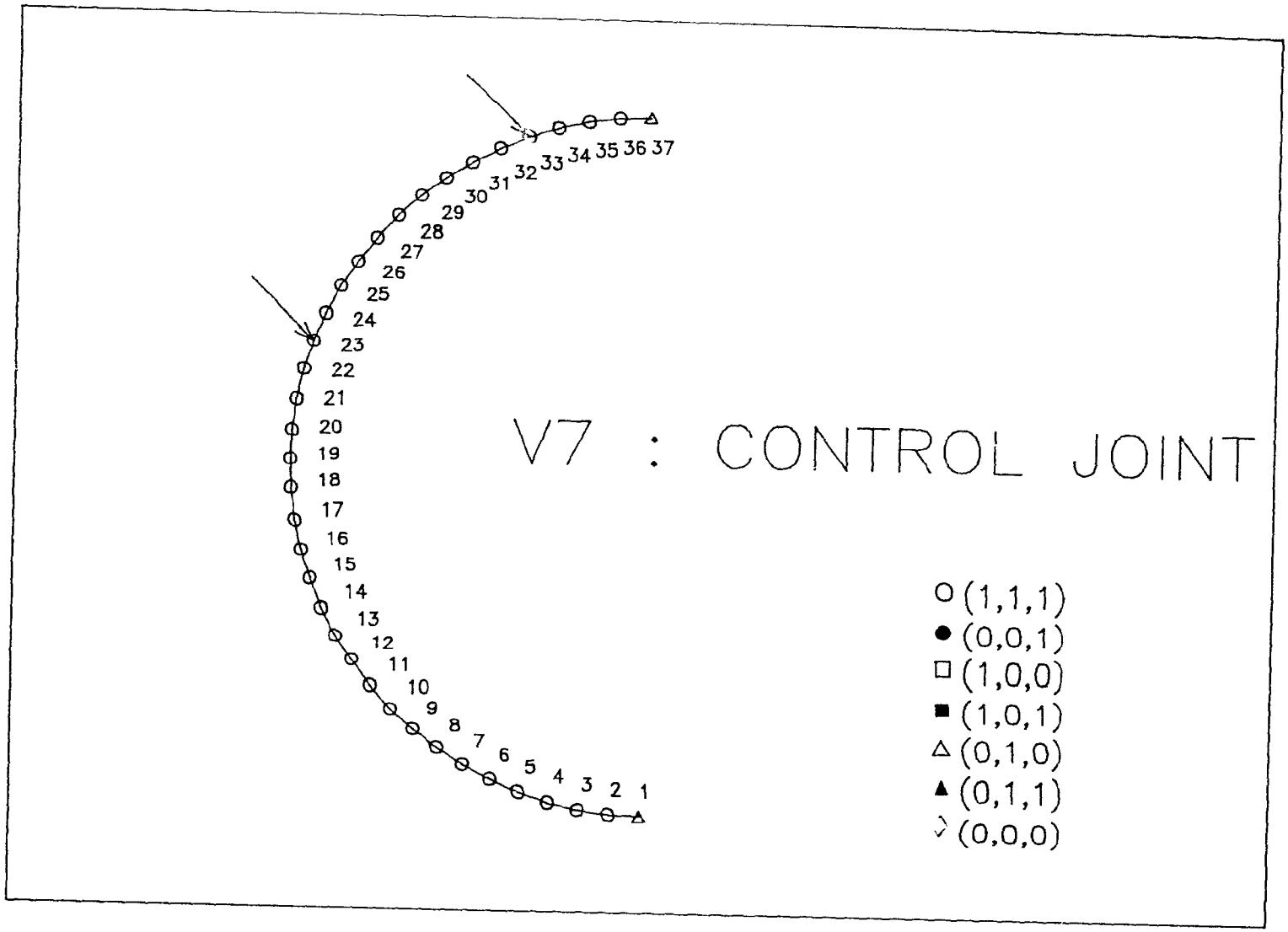

Figure 5.2 Sample DATACK Graphical Output.

During the non-linear analysis successive load increments and iterations are displayed to keep the user informed of the solution progress and speed.

5.3.4 PENLOAD

PENLOAD can calculate the load-deformation curves of up to seven data files simultaneously. These input files can either be the TUB DIS files from TUBE2D or EXP.DIS files containing the experimental load-deformation data directly If the input files contain data with different measurement units, or coming from specimens with different yield stresses, for example, the data can be normalized using the load factors which PENLOAD prompts for Similary the user will be asked to supply multiplication factors for deformation scaling. Finally PENLOAD prompts the user for title, axis labels and legend location All the load-deformation graphs of Chapter 4 were output by PENLOAD.

5.3.5 SHAPE

The program SHAPE displays the deformed cross-sections and the corresponding load. The load can be either in kN or in Kips as selected by the user For the purposes of clarity the displacements can be magnified as desired by the user and the magnification factor will be displayed. The users also choose display mode 1, 2 or 4 to see the cross-sections individually, two or four at a time. The number of cross-sections displayed need not be a multiple of the display mode A sample screen is shown in Fig. 5.3.

5.3.6 VIEW

The VIEW utility from the FORTPLOT library is used to store graphical files and recall them when required. All graphical hardcopies are output through the VIEW utility. VIEW is another module where prompts are few and are limited to input and output devices.

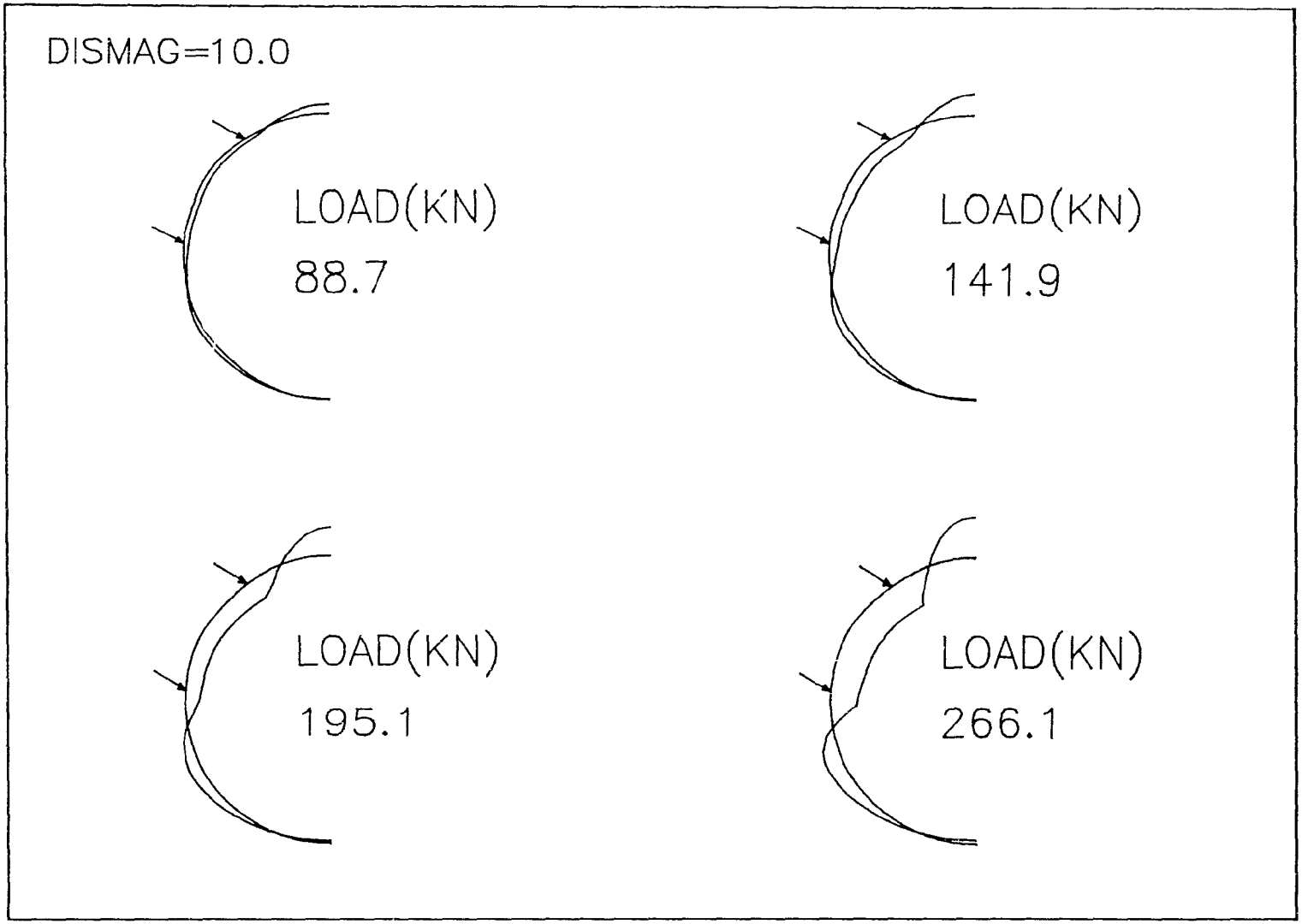

Figure 5.3 Sample SHAPE Graphical Output.

CHAPTER 6

CONCLUSIONS

6.1 Conclusions

The following conclusions can be drawn from the experimental and theoretical investigations presented in this report:

1. The common practice of treating V-joints as two separate T-joints is generally conservative for 90° V-joints but cannot be relied on for joints with different out-of-plane angles between the branches.
2. It was observed that while the 90° V-joints were three to four times stiffer than comparable T-joints the 60° and 120° joints were only twice as stiff. The softening of the response was attributed to the tendency of the branches to ovalize the chord in the same sense whether on opposite sides of the chord or at the same side and separated by a small out of plane angle
3. An increase in strength was typically noted with the addition of a second branch at 90° to the first one. A decrease in strength was recorded for joints with $\phi > 90°$.
4. The AWS Code is the first one to directly address out of plane branches but the strength gain predicted by its formula is too optimistic.
5. All V-joint hotspots were located at the back of the joint, and were most often at the branch saddle intersection. Value of the stress concentration factors varied

from 0.5 to 2.5 times that of the comparable T-joints. Some similarities between T- and V-joints in the effect of the geometric ratios were noted, but were generally insufficient to fully predict V-joint response.

6. An elastic-plastic beam-column element supported by tangential and normal linear elastic continuous springs was used to develop a ring-type finite element model for simple tubular joints The load-deformation predictions for the 90° joints showed good agreement for most of the response curve. The predictions of the model for the more flexible V-joints were not in agreement with experimental results.
7. The effect of the test parameters was reflected in the computed load-deformation curves for T-joints but the predicted stiffnesses were always higher than those found experimentally
8. A deformation limit of 1% of the chord radius was suggested as a possible validity range for the analytical model.

6.2 Suggestions for Further Work

As reported in the introduction, this thesis presents the first data for a V-joint experimental database. More tests should be done to confirm the results and trends presented herein. In particular joints with ϕ between 90° and 120° could be tested to further define the combination of parameters which decrease the strength of V-joints to values below that of their comparable T-joints.

The shortcomings of the model might be overcome by the inclusion of non-linearity in the springs response as well as the inclusion of the geometric non-linearity in the beam-element response. These additions would soften the predicted response for the more flexible joints and enable the model to calculate a failure load.

LIST OF REFERENCES

1. Underwater Engineering Group, *Design of Tubular Joints for Offshore Structures*, Vols. 1, 2, 3, UEG Publication UR33, 1985
2. Scordelis, A. C., Bouwkamp, J. E., *Analytical Study of Tubular Tee-Joints*, Journal of the Structural Division, ASCE, Vol. 96, No. ST1, Jan. 1970, pp. 65-87.
3. Toprac, A. A., Johnston, L. P., Noel, J., *Welded Tubular Connections· An Investigation of Stresses in T-joints*, Supplement to the Welding Journal, Jan. 1966, pp. 1-12.
4. Marshall, P. W., *Connections for Welded Tubular Structures, Proceedings of Welding of Tubular Structures Conference*, International Institute of Welding, Boston, July 1984, pp. 1-54.
5. Kuang, J. E., Potvin, A. B , Leick, R. D., *Stress Concentration in Tubular Joints*, Proceedings of Offshore Technology Conference, Paper 2205, Houston, May 5-8, 1975, pp. 543-607.
6. Graff, J.W., Marshall, P W., Nimas, A.W., *Review of Design Considerations for Tubular Joints*, ASCE Preprint 81-043, New York, May 11-15, 1981
7. Chen, T. Y., Chen, B. Z., Wang, Y. Q., *The Stress Analysis and Experimental Research of Tubular Joints of Offshore Drilling Platform*, Journal of Energy of Research Technology, Vol 106, March 1984, pp. 43-45.
8. Irvine, M., Fessler, H., Wordsworth, A C., *Physical Model Stress Analysis of Steel Tubular Connections*, Offshore Structures· the Use of Physical Models in their Design, Ed Armer, G. S. T , Garas, F K., Lancaster: Construction Press, 1981
9. Visser, W., *On the Structural Design of Tubular Joints*, Proceedings of Offshore Technology Conference, Paper 2117, Houston, May 6-8, 1974, pp 881-894.
10. Gibstein, M. B., *Parametric Stress Analysis of T-Joints*, European Offshore Steel Research, Cambridge, Paper 26, 1978
11. Reber, J. B., *Ultimate Strength Design of Tubular Joints*, Journal of the Structural Division, ASCE, Vol. 99, No. ST6, June 1973, pp. 1223-1240.
12. American Petroleum Institute, *Recommended Practice for Planning, Designing and Constructing Fixed Offshore Platforms*, API RP2A, 15^{th} ed., 1984.
13. Irons, B.M., Sohrad, A., *Technique of Finite Elements*, Chichester, England, E. Horwood; New York, Halsted Press, 1980.
14. Stamenkovic, A., Sparrow, K D., *Load Interaction in T-Joints of Steel Circular Hollow Sections*, Journal of Structural Engineering, ASCE, Vol. 109, Sept. 1983, pp. 2192-2205
15. Brebbia, C A., *Finite Element Systems: A Handbook*, Southhampton, Hampshire; Computational Mechanics Center; Berlin, Springer-Verlag, 1985.

LIST OF REFERENCES *(Continued)*

16. Toprac, A. A., Natarajan, M, Erzurumlu, H., Kanoo, A. L. J.,*Research in Tubular Joints: Static and Fatigue Loads*, Proceeding of Offshore Technology Conference, Paper 1062, Houston, May 18-21 1969, pp. 667-680.
17. Yamasaki, T., Takizawa, S., Komatsu, M., *Static and Fatigue Tests on Large Size Tubular Joints*, Proceedings of Offshore Technology Conference, Paper 2434, Houston, April 30 - May 3, 1979, pp. 583–591.
18. Yura, J. A., *Connections with Round Tubes*, Proceedings of Symposiums on Hollow Structural Sections in Building Structures, ASCE, Chicago, Sept. 15-17 1985, pp. 5-1, 5-18.
19. American Welding Society, *Structural Welding Code – Steel – AWS D1.1*, 10^{th} ed., 1985.
20. Yura, J. A., Zettlemoyer, N., Edwards, I E., *Ultimate Capacity of Tubular Joints*, Journal of Structural Division, ASCE, Vol. 107, No. St10, Oct. 1981, pp. 1965-1982.
21. Wardenier, J., *The Strength of Predominantly Statically Loaded Joints in the Offshore Structures*, PATO Offshore Course, Dec. 1984, 20 pp.
22. Billington, C. J., Lalani, M., Tebbett, I. E., *Background to New Formulas for the Ultimate Limit State of Tubular Joints*, Journal of Petroleum Technology, APIM, Vol. 37, No. 1, Jan 1984, pp. 147-156.
23. Kurobane, Y., Makino, Y., Mitsui, Y., *Ultimate Strength Formula for Simple Tubular Joint*, IIW Doc XV-385-76.
24. Kurobane, Y., Makino, Y., Mitsui, Y., *Re-analysis of Ultimate Strength Data for Truss Connections in Circular Hollow Sections*, IIW Doc XV-461-80.
25. Kurobane, Y., *Recent Developments in Tubular Joint Design*, Preprint 81-002, ASCE, New York, May 11-15, 1981.
26. Ochi, K., Makino, Y., Kurobane, Y., *Basis for Design of Unstiffered Tubular Joints under Axial Brace Loading*, IIW Doc XV-561-84.
27. Dijkstra, O. D., de Back, J., *Fatigue Strength of Tubular T- and X-Joints*, Offshore Technology Conference, Paper 3696, Houston, May 5-8 1980, pp. 177-186.
28. Wordsworth, A. C., Smeldley, E. P., *Stress Concentration of Unstiffered Tubular Joints*, European Offshore Steel Research Seminar, Paper 31, Cambridge, 1978.
29. Recho, N., Brozetti, J., *Stress Concentration at Tubular V-Joints*, Proceedings of Welding of Tubular Structures Conference, International Institute of Welding, Boston, July 1984, pp 517-524.
30. Mitri, H. S., *Program NAF2D: Nonlinear Analysis of Frames in 2 Dimensions*, Structural Engineering Series No. 85-3, McGill University, Montreal, 1985.

LIST OF REFERENCES *(Continued)*

31. Mitri, H. S., Scola, S., Redwood, R. G., *Experimental Investigation into the Behaviour of Axially Loaded Tubular V-Joints*, Proceedings of CSCE Centennial Conference, Structures Division, CSCE, Vol. 1, Montreal, May 19–22, 1987, pp. 397-410.

32. Merlo, J. A., *A Study of Separated Double Chord T-joints for HSS Trusses*, M.Eng Thesis, McMaster University, Hamilton , 1987.

33. American Society for Testing Materials, Volume 1.04 Section A370, 1985.

34. Technical Memorandum of Column Research Council, Stub Column Test Procedures, pp. 559-567.

35. McGill Plotting Package, McGill University Computing Center, *Graphics User's Manual*, Shawn Wasser, Montreal, Nov 1983.

36. Jeffrey, D. A., *FORTPLOT Library*, University of Western Ontario, 1986.

APPENDIX A

MEASURED SPECIMEN DIMENSIONS

Table A. 1 Chord Thicknesses

Specimen	Nominal	Measured	Measured	Measured	Average
T1	4.78	4.95	4.95	4.98	
		4.93	4.90	4.93	4.94
T2	8.18	8.225	8.23	8.20	
		8.20	8.18	8.18	8.21
T3	6.35	6.375	6.40	6.43	
		6.375	6.375	6.43	6.40
T4	6.35	6.43	6.40	6.35	
		6.35	6.375	6.30	6.37
T5	6.35	6.43	6.40	6.375	
		6.40	6.43	6.30	6.39
ST6	6.35	6.43	6.45	6.375	
		6.375	6.375	6.30	6.38
V1	4.78	4.93	4.93	4.95	
		4.90	4.90	4.93	4.92
V2	8.18	8.28	8.255	8.255	
		8.23	8.23	8.20	8.24
V3	6.35	6.35	6.30	6.35	
		6.27	6.30	6.32	6.315
V4	6.35	6.35	6.375	6.40	
		6.30	6.325	6.30	6.34
V5	6.35	6.45	6.35	6.40	
		6.40	6.32	6.43	6.39
V6	6.35	6.40	6.375	6.45	
		6.32	6.375	6.43	6.39
V7	6.35	6.27	6.30	6.27	
		6.48	6.30	6.32	6.32
V8	6.35	6.375	6.25	6.30	
		6.30	6.30	6.27	6.30
DT1	6.35	6.30	6.27	6.32	
		6.30	6.30	6.32	6.30

Table A. 2 Chord Diameters, D1

Specimen	Inner Diameter	Average	$2 \times T$	D_1
T1	209.4, 209.3, 209.5	209.40	9.88	219.3
T2	202.5, 203.3, 203.7	203.17	16.42	219.6
T3	205.3, 207.6, 207.8	206.90	12.80	219.7
T4	206.5, 207.1, 208.3	207.32	12.74	220.1
T5	207.4, 206.3, 207.1	206.93	12.78	219.7
T6	207.4, 207.8, 207.0	207.40	12.76	220.2
V1	210.6, 209.9, 208.8 209.9, 210.3, 209.3	209.89	9.84	219.6
V2	203.5, 203.7, 203.4 203.4, 202.9, 203.3	209.89	9.84	219.6
V3	207.4, 206.9, 207.3 207.2, 207.8, 207.9	207.33	12.63	220.0
V4	206.5, 207.2, 206.9 207.5, 207.5, 207.4	207.16	12.68	219.8
V5	208.7, 206.3, 208.0 207.8, 206.5, 206.1	207.23	12.78	220.0
V6	206.7, 207.4, 206.0 205.5, 207.7, 207.5	206.92	12.78	219.7
V7	207.6, 207.6, 208.0 206.9, 207.1, 207.3	207.42	12.64	220.1
V8	205.0, 208.5, 207.0 207.1, 207.0, 207.9	207.08	12.60	219.7
DT1	207.2, 208.0, 207.1 209.0, 205.7, 207.6	207.43	12.60	220.0

Table A. 3 Average Chord Diameters

Specimen	Circumference	Average (πD)	D_2	D_1	$\frac{(D_1+D_2)}{2}$
T1	692, 693	692.5	220.4	219.3	219.85
T2	692, 692	692.0	220.3	219.6	219.95
T3	693, 691	692.0	220.3	219.7	2220.00
T4	693, 692	692.5	220.4	220.1	220.25
T5	692, 691	691.5	220.1	219.7	219.60
T6	692, 694	693.0	220.6	220.2	220.40
V1	692, 692	692.0	220.3	219.6	219.95
V2	693, 692	692.5	220.4	219.6	220.00
V3	692, 693	692.5	220.4	220.0	220.25
V4	694, 694	694.0	220.9	219.8	220.35
V5	693, 394	693.5	220.8	220.0	220.40
V6	691, 692	691.5	220.1	219.7	219.90
V7	693, 695	694.0	220.9	220.1	220.50
V8	693, 694	693.5	220.8	219.7	220.25
DT1	693, 692	692.5	220.4	220.0	220.20

Table A. 4 Average Branch Diameters

Specimen	Nominal d	Circumference	Average	d
T1	88.9	279, 280	279.5	89.0
T2	88.9	280, 281	280.5	89.3
T3	141.3	446, 445	445.5	141.8
T4	48.3	152, 154	153.0	48.7
T5	88.9	280, 279	279.5	89.0
T6	168.3	531, 531	531.0	169.0
V1	88.9	280, 280	280.0	89.1
V2	88.9	280, 281	280.5	89.3
V3	141.3	447, 447	447.0	142.3
V4	48.3	153, 155	154.0	49.0
V5	88.9	282, 281	281.5	89.6
V6	88.9	281, 280	280.5	89.3
V7	88.9	282, 282	282.0	89.8
V8	168.3	532, 532	532.0	169.3
DT1	88.9	280, 281	280.5	89.3

APPENDIX B

STRESS STRAIN CURVES FOR 6.35 mm CHORD

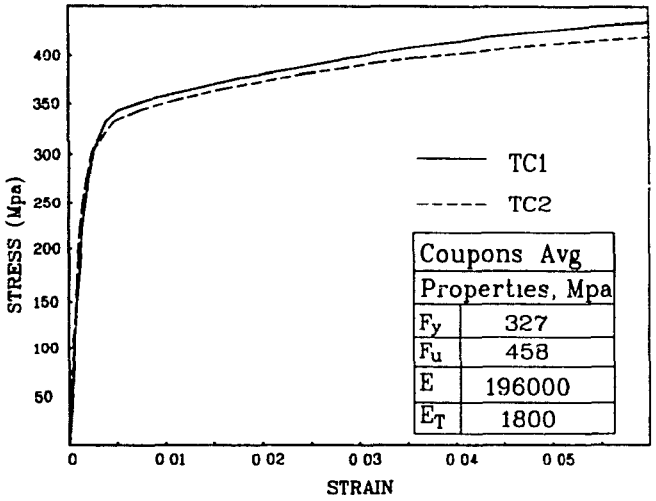

(a) Tensile Coupons Properties

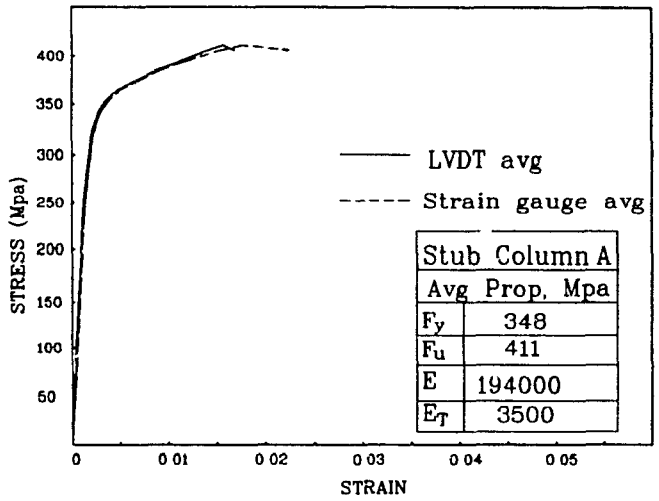

(b) Stub Column 6.35A Properties

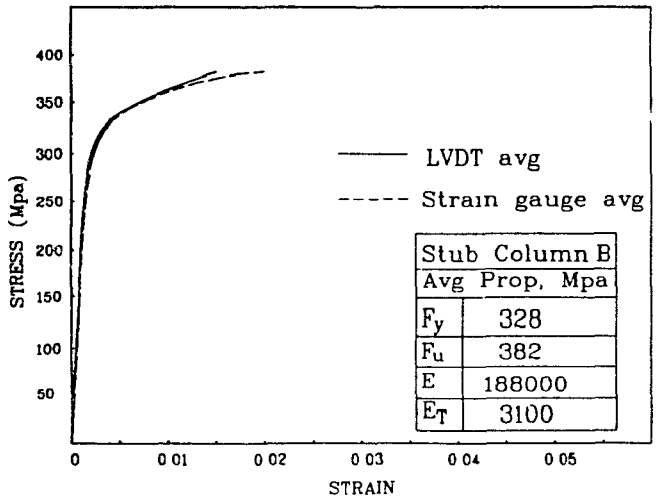

(c) Stub Column 6.35B Properties

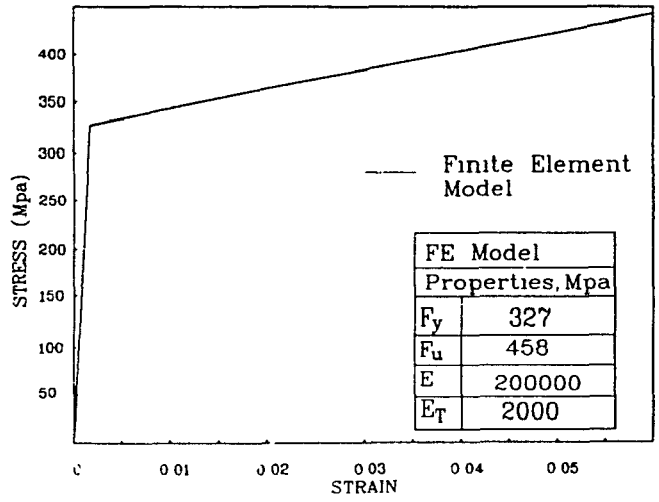

(d) Finite Element Model Properties

Figure B.1 Stress Strain Curves for Material with Chord Thickness 6.35 mm.